A Spectroscopic Description of Asymmetric Isotopologues of CO_2

M. Bermúdez-Montaña[1], M. Rodríguez-Arcos[2], M. Carvajal[3,4],
C.Ostertag-Henning[5], and R. Lemus*[6]

[1] Tecnologico de Monterrey, Escuela de Ingeniería y Ciencias, Carr. al Lago de Guadalupe Km. 3.5, Atizapán de Zaragoza 52926, Estado de Mexico, Mexico
[2] School of Engeneering and Science, Tecnológico de Monterrey, Ave. Eugenio Garza Sada 2501, 64849 Monterrey, NL, Mexico
[3] Dpto. Ciencias Integradas, Centro de Estudios Avanzados en Física, Matemáticas y Computación, Unidad Asociada GIFMAN, CSIC-UHU, Universidad de Huelva, 21071 Huelva, Spain
[4] Instituto Universitario "Carlos I" de Física Teórica y Computacional, Universidad de Granada, Spain
[5] Federal Institute for Geosciences and Natural Resources, Germany
[6] Instituto de Ciencias Nucleares, UNAM. A.P.70-543, Circuito Exterior, C.U. 04510 Mexico, CDMX, Mexico

*R. Lemus.
email: renato@nucleares.unam.mx
Phone: +52 55 58058099

Abstract

A polyad-conserving algebraic model applied to vibrational excitations of the asymmetric isotopologues of CO_2 is presented. First the problem of vibrational excitations is studied by taking into account only the minimum subspace of states to characterize the Fermi interaction. This analysis allows an estimation of the force constants as well as the feasibility of describing the system in a local mode scheme, in terms of $SU(2)$-operators associated with Morse ladder operators for the stretches. This description together with the algebraic $U(3)$ for the bends establishes the dynamical group $SU_1(2) \times U(3) \times SU_2(2)$ for the series of isotopologues. Six isotopologues are considered, namely $^{16}O^{12}C^{18}O$, $^{16}O^{12}C^{17}O$, $^{16}O^{13}C^{18}O$, $^{16}O^{13}C^{17}O$, $^{17}O^{13}C^{18}O$ and $^{17}O^{12}C^{18}O$ in their electronic ground states. For the isotopologues $^{16}O^{12}C^{18}O$, $^{16}O^{12}C^{17}O$, $^{17}O^{12}C^{18}O$, and $^{16}O^{13}C^{18}O$, the vibrational description was carried out using a Hamiltonian involving 14 parameters. For this series of isotopologues with a number of energy terms $90, 57, 42$ and 40, the deviations obtained were rms=0.15, 0.10, 0.06 and 0.07 cm^{-1}, respectively. For $^{16}O^{13}C^{17}O$, with 28 experimental energies and involving 13 parameters, the deviation was rms=0.05 cm^{-1} while, for $^{17}O^{13}C^{18}O$, a different strategy was proposed since only 12 experimental energy levels. In all cases the polyad scheme $P_{212} = 2(\nu_1 + \nu_3) + \nu_2$ was considered. In addition, a new criterion of locality/normality degree is proposed, embracing the case of molecules with normal mode behavior, in particular, the isotopologues of CO_2.

Keywords: Algebraic approach, vibrational excitations, asymmetric isotopologues of CO_2, polyad-conserving scheme.

1 Introduction

Beyond the unquestionable importance of the CO_2 molecule in the chemistry of the Earth's environment, this molecule is also significant because it has been detected in the atmosphere of other planets as well as in the exterior space and it is used as a tracer of the evolution of stars [1, 2, 3, 4, 5, 6, 7]. Human industrial activity is responsible for the alarming increase of this greenhouse gas, being the atmospheric CO_2 the central contribution in the global warming [8, 10, 11, 12]. This fact together with the advances in spectroscopic techniques have lead to a large augmentation of experimental analysis with the purpose of establishing a complete and accurate characterization of CO_2 and its isotopologues [13, 14, 15, 16, 17, 18, 19, 20, 21, 23, 24, 25, 26, 27, 28, 29, 30, 31, 32, 33, 34, 35, 36, 37, 38, 39, 40, 41, 42, 43, 44, 45, 46, 47, 48, 50, 51]. In spite to the great amount of ongoing experimental spectroscopic information on the isotopologues of CO_2, for some of them very few experimental vibrational energies have been reported, in particular for (838), (737) and (738) (in simplified notation, $^{17}O^{13}C^{18}O \rightarrow$ (738), for instance). Given the profuse spectroscopic data, theoretical models can be tested in different fronts. A precise theoretical description may be of great importance to provide a feedback to the experimentalists in the search of line assignment, but also to test and improve the models providing additional physical insights about the systems. In particular, the experimental techniques involving highly excited states of the ro-vibrational degrees of freedom demand theoretical treatments in the field of high resolution spectroscopy. In this venue, the rotational description is usually carried out through a perturbative approximation of the Hamiltonian [52, 53, 54, 55, 56, 58]. On the other hand, variational approaches address both spectra and potential energy surface to study the nuclear dynamics [59, 60, 61, 62, 63, 64, 65, 66, 67, 68, 69, 70, 71, 72, 73, 74] as well as the dipole moments in case we were interested in the simulation of the infrared spectra [64, 75, 76, 77, 78, 79, 80]. Regarding the description of the isotopologues of CO_2, the work of *Huang et al* deserves particular attention due to the comprehensive study of them [65]. Within the Born-Oppenheimer approximation the potential energy surface is the same for every isotopologue, a fact that establishes relations between their frequencies [81]. Concerning this point the determination of the abundances has received much attention in the last years due, in part, to the fact that it is now possible to make accurate measures to determine low natural abundances [60, 82, 83, 84, 85, 86, 87, 88, 89, 90, 91]. Gas phase mass spectrometry represents the first option to identify abundances, but it presents limitations that impedes their determination of all the isotopologues [92, 93] despites the advances in high resolution mass spectrometry permits the differentiation of the isotopologues (627) and (636) [94]. The difficulty in determining the relative abundances has motivated scientists to a search for alternatives represented by IR and Raman spectroscopy [95, 96, 97]. These analytical tools involve a detailed study of the vibrational degrees of freedom to provide the wave functions, a fundamental ingredient for the simulations of IR and Raman spectra.

The study of the principal isotopologue $^{12}C^{16}O_2$ has been developed using an algebraic approach based on the dynamical group $SU_1(2) \times U(3) \times SU_2(2)$ since 14 years ago. This study was first carried out paying attention to the vibrational excitations [98, 99, 100, 101] and, later on, focusing on the simulation of the Raman spectrum [102, 103, 106]. More recently we started a systematic study of the vibrational excitations of the symmetric isotopologues of carbon dioxide $^{13}C^{16}O_2$, $^{12}C^{18}O_2$ and $^{12}C^{17}O_2$ in their electronic ground states [107]. The description was again approached using the algebraic model $SU_1(2) \times U(3) \times SU_2(2)$, which consists in considering Morse potentials for the stretches [108, 109, 110, 111] and the 2D-vibron model for the bends [112, 113]. In this contribution we present the study of the asymmetric isotopologues in the framework of the same scheme. Surprisingly, the description of the asymmetric series turned out to be somewhat more involved due to the fact that the symmetry adapted coordinates do not coincide with the normal coordinates and, consequently, a treatment involving the GF formalism should be introduced [114]. We shall show that, in this case, a suitable basis set is obtained considering the same symmetry adapted coordinates used for the symmetric isotopologues, a fact that allows the symmetric limit to be recovered in natural form. The convenience of this basis is proved through the estimation of force constants when compared with the normal modes.

The carbon dioxide and its isotopologues have a strong normal mode behavior. This fact makes them ineligible to be analyzed in the context of the traditional study of local modes, where the local coordinates are assigned to the stretching degrees of freedom [115, 116, 117, 118, 119, 120, 121, 122]. In contrast we propose a criterion based on a model of harmonic oscillators keeping the connection between the normal and local bosonic operators through a Bogoliubov transformation [123, 124]. This

transformation provides the key to introduce a measure of the degree of normality/locality for any set of equivalent oscillators beyond the type of behavior of a given molecule. This procedure allows the connection between a Hamiltonian given in terms of normal modes and a Hamiltonian in terms of local oscillators. The importance of establishing this connection is crucial in our algebraic method since it is through the local representation that we propose a mapping from bosonic harmonic oscillators to $SU(2)$-Morse ladder operators for the stretches and $U(3)$-ladder operators for the bends. This anharmonization procedure allows us to improve the vibrational descriptions in a local scheme even in molecules with a clear normal mode behavior.

The general scheme of our approach consists in expanding both the kinetic and potential contributions up to cubic terms just to include the Fermi interaction characterizing these molecules [125]. The next step consists in introducing an algebraic representation invoking the connection between the bosonic operators and the normal coordinates and momenta. An algebraic representation in terms of local operators is obtained through a canonical transformation. The final algebraic representation of the Hamiltonian is then improved by adding interactions of higher order in purely algebraic form. The goal of our model is to establish an effective Hamiltonian with a minimum number of parameters capable of providing high quality vibrational descriptions.

In our description the polyad $P_{212} = 2(\nu_1 + \nu_3) + \nu_2$ is considered. For the principal isotopologue alternative polyad schemes have been used. *McCoy and Sibert* III [126] used the polyad $P_{214} = 2\nu_1 + \nu_2 + 4\nu_3$, while polyad $P_{213} = 2\nu_1 + \nu_2 + 3\nu_3$ is in general used in the context of variational methods [60] as well as in effective Hamiltonians [14]. For the isotopologues under study the three polyads may be tested. However, based on the assessment of the three polyads carried out through the comparison between the experimental and the simulated Raman spectra in $^{12}C^{16}O_2$, where the polyad P_{212} was considered as the best option, we chose this latter polyad in our description, previously used with good results [99, 100, 101, 102, 103].

This paper is organized as follows. In Section 2, the local-to-normal transition is analyzed from the point of view of the estimation of the force constants. Here a criterion to assign a degree of locality/normality is introduced. Section 3 is devoted to present the Hamiltonian associated with polyad P_{212}. In Section 4, the vibrational analyses obtained for the six asymmetric isotopologues are presented. Finally, the conclusions are drawn in Section 5. An appendix is added where the case of the limit of symmetric isotopologues is discussed.

2 Local-to-normal mode transition

For the description of the vibrational degrees of freedom a crucial ingredient is the selection of the coordinates used to obtain the Hamiltonian. In our case we are interested in a local mode description because this is the appropriate way to introduce the mapping to anharmonic oscillators. Hence, the model must be given in terms of internal coordinates, although starting from a scheme of normal modes. In this process we shall introduced an intermediate step in terms of the symmetry adapted coordinates used for symmetric isotopologues. This proposal turns out to be close to the normal modes as it will be proved through the estimation of the force constants. In addition, we connect the normal and the local mode descriptions leading to a criterion to establish the degree of normality/locality for the series of asymmetric isotopologues. This criterion helps to provide a correlation between the components of the wave functions and the degree of normality/locality. We start with the vibrational description in terms of local coordinates. Although, at first sight, this analysis resembles an exercise of textbook, it is relevant to justify our selection of the basis as well as to establish our normal/local degree criterion.

2.1 Description in terms of local internal coordinates

Due to the preponderance of the Fermi resonance in these systems it is clear that even the simplest model must include the Fermi interaction. Hence we start considering the simplest Hamiltonian up to cubic interactions plus the Fermi interaction.

The Hamiltonian in configuration space of two non-equivalent interacting oscillators plus the bending and Fermi contributions is given by

$$\hat{H}^{(\mathrm{L})} = \hat{H}^{(\mathrm{L})}_{[2]} + \hat{V}^{(\mathrm{L})}_{F}, \tag{1}$$

where

$$\hat{H}^{(\mathrm{L})}_{[2]} = \sum_{i=1}^{2}\left(\frac{1}{2}g^{(0)}_{ii}p_i^2 + \frac{1}{2}f_{ii}q_i^2\right) + g^{(0)}_{12}\ p_1p_2 + f_{12}\ q_1q_2 + \frac{1}{2}g^{(0)}_{aa}(p_a^2+p_b^2) + \frac{1}{2}f_{aa}(q_a^2+q_b^2), \tag{2}$$

and

$$\begin{aligned}\hat{V}^{(\mathrm{L})}_F =& \frac{1}{2}\left(\frac{\partial g_{aa}}{\partial q_1}\right)_0 q_1(p_a^2+p_b^2) + \frac{1}{2}\left(\frac{\partial g_{aa}}{\partial q_2}\right)_0 q_2(p_a^2+p_b^2)\\ &+ \frac{1}{2}\left(\frac{\partial g_{1a}}{\partial q_a}\right)_0 [p_1(q_ap_a+q_bp_b)+H.c.]\\ &+ \frac{1}{2}\left(\frac{\partial g_{2a}}{\partial q_a}\right)_0 [p_2(q_ap_a+q_bp_b)+H.c.]\\ &+ \frac{1}{2!}[f_{1aa}(q_1+q_2)(q_a^2+q_b^2)].\end{aligned} \tag{3}$$

where $q_i = r_i - r_e$ $(i = 1, 2)$ are the internal displacement coordinates with associated momenta p_i for the stretches, while $\{q_a, q_b\}$ are the Cartesian bending coordinates and their conjugate momenta $\{p_a, p_b\}$ [104, 105]. The coefficients $g^{(0)}_{ij}$ and f_{ij}, f_{1aa} correspond to the Wilson matrix elements evaluated at equilibrium and the force constants, respectively. Using the transformations given in the Appendix A, the Hamiltonian (1) can be recasted in the following algebraic form

$$\begin{aligned}\hat{H}^{(\mathrm{L}')} =& \hbar\omega_g\ a_g^\dagger a_g + \hbar\omega_u\ a_u^\dagger a_u + \hbar\omega \sum_{\alpha=+,-}\tau_\alpha^\dagger\tau_\alpha\\ &+ \delta_{gu}(a_g^\dagger a_u + a_g a_u^\dagger)\\ &+ \alpha_g^{(\mathrm{L}')}(a_g^\dagger\tau_+\tau_- + H.c.) + \alpha_u^{(\mathrm{L}')}(a_u^\dagger\tau_+\tau_- + H.c.),\end{aligned} \tag{4}$$

where

$$\begin{aligned}\alpha_g^{(\mathrm{L}')} =& \frac{1}{4}\left[\left(\frac{\partial g_{aa}}{\partial q_1}\right)_0 + \left(\frac{\partial g_{aa}}{\partial q_2}\right)_0\right]\hbar\omega\mu\sqrt{\frac{\hbar}{\omega_g\mu_g}}\\ &- \frac{\hbar}{2}\left[\left(\frac{\partial g_{1a}}{\partial q_a}\right)_0 + \left(\frac{\partial g_{2a}}{\partial q_a}\right)_0\right]\sqrt{\hbar\omega_g\mu_g}\\ &- \frac{1}{2!}\frac{\hbar}{\omega\mu}\sqrt{\frac{\hbar}{\omega_g\mu_g}}\ f_{1aa},\end{aligned} \tag{5}$$

and

$$\alpha_u^{(\mathrm{L}')} = -\frac{\gamma}{4}\hbar\omega\mu\sqrt{\frac{\hbar}{\omega_u\mu_u}}; \qquad \delta_{gu} = \frac{\hbar}{8}r_e\gamma\sqrt{\frac{\omega_g\omega_u}{G^{(0)}_{gg}G^{(0)}_{uu}}}. \tag{6}$$

The introduction of the realizations (71) and (72) implies that the Hamiltonian we are considering does not correspond to a local algebraic representation. In fact, it corresponds to a representation in terms of normal modes of the symmetric isotopologues. Nevertheless, as this Hamiltonian is originally expressed in local coordinates, it is labeled with the superindex (L'). On the other hand, this set of coordinates allows the identification of two specific contributions for the asymmetric isotopologues. They are the interactions associated with the coefficients δ_{gu} and $\alpha_u^{(\mathrm{L}')}$ that contain the ungerade operators $a_u^\dagger(a_u)$. Because we are interested in comparing the force constants derived from (4) and the corresponding Hamiltonian in terms of normal modes, where only four interactions are involved, we consider only the following states

$$\Sigma^+ : a|10^00\rangle + b|02^00\rangle, \tag{7}$$

$$\Sigma^+ : b|10^00\rangle - a|02^00\rangle, \tag{8}$$

$$\Sigma^+ : |00^01\rangle, \tag{9}$$

$$\Pi^\pm : |01^10\rangle. \tag{10}$$

which allow to determine the force constants $\{f_{11}, f_{12}, f_{aa}, f_{1aa}\}$. However the Hamiltonian (4) involves six interactions from which these four constants are to be obtained. In principle we need two more states to determine the six parameters. Since we are interested in evaluating the importance of choosing the symmetry adapted coordinates, not in obtaining a good fit (for the moment), we shall neglect the contributions δ_{gu} and $\alpha_u^{(\mathrm{L'})}$. In this way we are able to estimate the force constants using the four states listed above. Later on, these results will be compared with the ones provided in the framework of normal modes. Following this approach we obtain the parameters displayed in Table 1 , from which we have estimated the force constants displayed in Table 2. As a reference we have included the force constants obtained by *Sánchez-Castellanos et al* [100], where interactions up to quartic order are compared with *Chedin & Teffo*[72, 73], whose consider terms up to sextic order. This comparison permits to conclude the convenience of the symmetry adapted coordinates. However, it should be highlighted that the correct analysis of the asymmetric isotopologues must be done in terms of normal modes, a task to be done in the next section. Before proceeding to accomplish this task, it is worth stressing that we may carry out in straightforward way the analogue predictions of the force constants for the symmetric isotopologues, presented in the Appendix B.

Table 1: Parameters in cm^{-1} obtained by fitting the four states (7-10) using the Hamiltonian (4) with $\delta_{gu} = \alpha_u^{(\mathrm{L'})} = 0$.

Isotopologue	ω_g	ω_2	ω_u	$\alpha_g^{(L')}$
(637)	1318.97	645.74	2274.09	-47.96
(638)	1300.51	643.33	2265.97	-48.19
(627)	1318.87	664.72	2340.01	-51.61
(628)	1300.52	662.37	2332.11	-51.81
(728)	1280.85	659.69	2322.44	-52.09

Table 2: Local force constants estimated from the spectroscopic constants displayed in Table 1 using the relations (73,74) and (5).

Isotopologue	$f_{11}^{(L')}(aJ\mathring{A}^{-2})$	$f_{12}^{(L')}(aJ\mathring{A}^{-2})$	$f_{aa}^{(L')}(aJ\mathring{A}^{-2})$	$f_{1aa}^{(L')}(aJ\mathring{A}^{-3})$
(637)	15.55	1.35	0.57	-0.91
(638)	15.55	1.35	0.57	-0.90
(627)	15.54	1.35	0.57	-0.93
(628)	15.54	1.35	0.57	-0.94
(728)	15.54	1.35	0.57	-0.96
(626) Sánchez-Castellano[100]	15.95	1.24	0.58	-0.96
(626) Chedin[72]	15.97	1.25	0.58	-0.88

2.2 Normal mode scheme

Since the Hamiltonian (2) is quadratic, it can be reduced to a diagonal form by introducing the normal modes. In the case of the asymmetric isotopologues, both stretching local modes carry the same irreducible representation and, consequently, a symmetry adapted basis does not simplify the Hamiltonian to a diagonal form as in the case of the symmetric isotopologues. Hence we invoke the **GF** formalism to obtain the normal mode scheme.

The normal modes can be defined in terms of the internal coordinates using the transformation $\mathbf{L}$ matrix by

$$\mathbf{L}^{-1}\mathcal{G}_0\mathcal{F}\mathbf{L} = \mathbf{\Lambda}, \tag{11}$$

where the matrices $\mathcal{G}_0$ and $\mathcal{F}$ are given in terms of the symmetry adapted coordinates $\mathbf{S} = \{S_g, S_u\}$. It is convenient to notice that the condition $\mathbf{L}^{\dagger}\mathcal{G}_0^{-1}\mathbf{L} = \mathbf{1}$ provides the normalization of $\mathbf{L}$ after the diagonalization (11). The selection of symmetry adapted coordinates allows to establish the limit for

the symmetric isotopologues

$$\lim_{g_{22}^{(0)}\to g_{11}^{(0)}} \mathcal{Q}_1 \to \quad \frac{1}{\sqrt{g_{11}^{(0)}+g_{12}^{(0)}}}\, S_g \tag{12}$$

$$\lim_{g_{22}^{(0)}\to g_{11}^{(0)}} \mathcal{Q}_2 \to \quad \frac{1}{\sqrt{g_{11}^{(0)}-g_{12}^{(0)}}}\, S_u. \tag{13}$$

Imposing this limit, the phases involved in the diagonalization are fixed. We may now proceed to express the Hamiltonian (1) in normal coordinates. Before accomplishing this task we should recall that the limits (12) and (13) imply that we have chosen the first stretching mode to be in resonance with the bending mode according to the symmetry. We can thus neglect the Fermi interaction of the bending mode involving the second normal mode. Taking into account these considerations the Hamiltonian (1) is written as

$$\hat{H}^{(\mathrm{N})}_{[2]} = \frac{1}{2}\{\mathcal{P}_1^2+\lambda_1\mathcal{Q}_1^2\}+\frac{1}{2}\{\mathcal{P}_2^2+\lambda_2\mathcal{Q}_2^2\}-g_{aa}P_+P_- - f_{aa}Q_+Q_-, \tag{14}$$

while the Fermi interaction is

$$\hat{V}_F^{(\mathrm{N})} = \alpha_1^F\mathcal{Q}_1P_+P_- + \alpha_2^F[\mathcal{P}_1(Q_-P_- + Q_+P_+) + H.c.] + \alpha_3^F[\mathcal{Q}_1Q_+Q_-], \tag{15}$$

with the definitions

$$\begin{aligned}
\alpha_1^F &= -\frac{1}{\sqrt{2}}\left[\left(\frac{\partial g_{aa}}{\partial q_1}\right)_0(L_{11}+L_{21})+\left(\frac{\partial g_{aa}}{\partial q_2}\right)_0(L_{11}-L_{21})\right]\\
\alpha_2^F &= \frac{1}{\sqrt{2}}\left(\frac{\partial g_{1a}}{\partial q_a}\right)_0(\tilde{L}^{-1})_{11}\\
\alpha_3^F &= -2\sqrt{2}\frac{1}{2!}f_{1aa}L_{11}.
\end{aligned} \tag{16}$$

Here the momenta $\mathcal{P}_\iota$ are associated with the normal coordinates. We now proceed to obtain the algebraic representation by introducing the bosonic operators $\mathcal{A}_\iota^\dagger(\mathcal{A}_\iota)$ associated with ι-normal mode

$$\mathcal{A}_\iota^\dagger = \frac{1}{\sqrt{2}}(\beta_\iota\mathcal{Q}_\iota - \frac{i}{\hbar\beta_\iota}\mathcal{P}_\iota); \qquad \mathcal{A}_\iota = \frac{1}{\sqrt{2}}(\beta_\iota\mathcal{Q}_\iota + \frac{i}{\hbar\beta_\iota}\mathcal{P}_\iota), \tag{17}$$

where $\beta_\iota^2 = \frac{1}{\hbar}(\lambda_\iota)^{1/2}$ with $\lambda_\iota = \Lambda_{\iota\iota}$. In terms of this transformation the algebraic representation takes the form

$$\hat{H}^{(\mathrm{N})} = \sum_{\iota=1}^{2}\frac{\hbar\Omega_\iota}{2}(\mathcal{A}_\iota^\dagger\mathcal{A}_\iota+\mathcal{A}_\iota\mathcal{A}_\iota^\dagger)+\hbar\omega\sum_{\alpha=+,-}\tau_\alpha^\dagger\tau_\alpha+\alpha_F\hat{V}_F^{(\mathrm{N})}, \tag{18}$$

where $\Omega_\iota = \lambda_\iota^{1/2}$, with the Fermi contribution as

$$\hat{V}_F^{(\mathrm{N})} = \alpha_F^{(\mathrm{N})}[\mathcal{A}_1^\dagger\tau_+\tau_- + H.c.], \tag{19}$$

and the spectroscopic parameter

$$\begin{aligned}
\alpha_F^{(\mathrm{N})} =& \frac{1}{4}\frac{\hbar\omega\mu}{\beta_1}\left[\left(\frac{\partial g_{aa}}{\partial q_1}\right)_0(L_{11}+L_{21})+\left(\frac{\partial g_{aa}}{\partial q_2}\right)_0(L_{11}-L_{21})\right]\\
&-\hbar^2\beta_1\left(\frac{\partial g_{1a}}{\partial q_a}\right)_0(\tilde{L}^{-1})_{11}-\frac{1}{2!}\frac{\hbar}{\beta_1\omega\mu}f_{1aa}L_{11}.
\end{aligned} \tag{20}$$

We have carried out a fit with the Hamiltonian (18) obtaining the spectroscopic parameters displayed in Table 3, which turn out to be the same as the ones given in Table 1. Indeed the difference between the local and the normal scheme comes up from the identification of the spectroscopic parameters with the structure and force constants [123, 124, 137]. From the fitted spectroscopic parameters given in Table 3 we calculated the force constants given in Table 4. We notice that, in general, the force constants are similar to the ones displayed in Table 2, a fact that validates the use of the symmetry adapted coordinates for the asymmetric isotopologues, chosen to describe the symmetric isotopologues. In fact, the normal coordinates turn out to be close to the symmetry adapted coordinates. This fact will help us to establish the mapping of the Hamiltonian (18) to an algebraic local representation as we present in the next subsection.

Table 3: Parameters in cm^{-1} obtained fitting the first three Σ^+ levels (7-9) and the bending fundamental ν_2 in the normal scheme using the Hamiltonian (18).

Isotopologue	ω_1	ω_2	ω_3	α_F
(637)	1318.97	645.74	2274.09	-47.96
(638)	1300.51	643.33	2265.97	-48.19
(627)	1318.87	664.72	2340.01	-51.61
(628)	1300.52	662.37	2332.11	-51.81
(728)	1280.85	659.69	2322.44	-52.09

Table 4: Force constants estimated in the normal mode scheme using the parameters displayed in Table 3.

Isotopologue	$f_{11}^{(N)}(aJ\AA^{-2})$	$f_{12}^{(N)}(aJ\AA^{-2})$	$f_{aa}^{(N)}(aJ\AA^{-2})$	$f_{1aa}^{(N)}(aJ\AA^{-3})$
(637)	15.55	1.35	0.55	-0.863
(638)	15.55	1.35	0.55	-0.875
(627)	15.54	1.35	0.54	-0.889
(628)	15.54	1.36	0.54	-0.913
(728)	15.54	1.36	0.54	-0.915
(626) Sánchez-Castellanos[100]	15.95	1.24	0.58	-0.96
(626) Chedin[72]	15.97	1.25	0.58	-0.88

2.3 Connection between the normal and local bosonic operators

We have presented two schemes to describe the vibrational excitations, namely, the local and normal mode descriptions. We next proceed to connect the Hamiltonian (18) with the local representation, a crucial task to improve the description by establishing a mapping of the local bosonic operators to Morse ladder operators. To accomplish this task we recall the expression of the bosonic operators $\mathcal{A}_\iota^\dagger(\mathcal{A}_\iota)$ associated with ι-normal mode (17) and introduce the transformation to symmetry adapted coordinates to obtain

$$\mathcal{A}_\iota^\dagger = \frac{1}{\sqrt{2}}\sum_\alpha \left\{\beta_\iota (L^{-1})_{\iota\alpha} S_\alpha - \frac{i}{\hbar\beta_\iota}(\tilde{L})_{\iota\alpha}\Pi_\alpha\right\}, \tag{21}$$

where S_α and Π_α are defined in (71) and (72). In order to establish the connection to the local description we introduce the local bosonic operators. To achieve this goal we introduce in (21) the definitions of the symmetry adapted coordinates in terms of the local coordinates. The result is

$$\mathcal{A}_\iota^\dagger = \frac{1}{2}\sum_\alpha \left\{\beta_\iota (L^{-1})_{\iota\alpha}(q_1 + (-1)^{(\alpha+1)}q_2) - \frac{i}{\hbar\beta_\iota}(\tilde{L})_{\iota\alpha}(p_1 + (-1)^{(\alpha+1)}p_2)\right\} \ , \tag{22}$$

where α is considered 1(2) for gerade(ungerade) stretching modes. We now take into account the algebraic realization

$$q_i = \frac{1}{\sqrt{2}}\sqrt{\frac{\hbar}{\omega_i\mu_i}}\left[a_i^\dagger + a_i\right]; \qquad p_i = \frac{i}{\sqrt{2}}\sqrt{\hbar\omega_i\mu_i}\left[a_i^\dagger - a_i\right], \tag{23}$$

to obtain

$$\mathcal{A}_\iota^\dagger = \sum_j (c_+^{\iota,j} a_j^\dagger + c_-^{\iota,j} a_j), \tag{24}$$

where

$$c_\pm^{\iota,j} = \frac{1}{2\sqrt{2}}\sum_\alpha (-1)^{(\alpha+1)(1-\delta_{j1})}\beta_\iota \sqrt{\frac{\hbar}{\omega_j\mu_j}}\left[(L^{-1})_{\iota\alpha} \pm (\tilde{L})_{\iota\alpha}\frac{\omega_j\mu_j}{\hbar\beta_\iota^2}\right]. \tag{25}$$

We should notice that the commutator $[\mathcal{A}_\iota, \mathcal{A}_\iota^\dagger] = 1$ implies the normalization

$$\sum_{j=1}^{2}(|c_+^{\iota,j}|^2 - |c_-^{\iota,j}|^2) = 1, \tag{26}$$

which, in fact, is satisfied. In Table 5 we present the results of these coefficients for the different isotopologues. From this table we notice that the main contributions to the operators $\mathcal{A}_\iota^\dagger$ correspond to the local creation operators albeit with different weights. Based on these results, if we neglect the

Table 5: Table of coefficients $c_\pm^{\iota,j}$ involved in the expansion (24) for the asymmetric isotopologues.

Isotopologue	$\iota-$th Mode	$c_+^{\iota,1}$	$c_+^{\iota,2}$	$c_-^{\iota,1}$	$c_-^{\iota,2}$	$\sum_j \lvert c_-^{\iota,j}\rvert^2$	δ_-
(637)	1	0.7156	0.7346	0.1619	0.1598	0.0518	0.0349
	2	0.7230	-0.7037	-0.0929	0.0968	0.0179	
(638)	1	0.7076	0.7434	0.1656	0.1617	0.0535	0.0359
	2	0.7315	-0.6957	-0.0919	0.0992	0.0182	
(627)	1	0.7182	0.7357	0.1700	0.1681	0.0572	0.0380
	2	0.7225	-0.7048	-0.0952	0.0989	0.0188	
(628)	1	0.7112	0.7439	0.1738	0.1702	0.0591	0.0392
	2	0.7302	-0.6970	-0.0943	0.1013	0.0192	
(728)	1	0.7208	0.7362	0.1762	0.1746	0.0615	0.0405
	2	0.7217	-0.7061	-0.0970	0.1003	0.0195	

contribution of the annihilation operators and normalize the coefficients we have

$$\mathcal{A}_\iota^\dagger \approx c_{N+}^{\iota,1} a_1^\dagger + c_{N+}^{\iota,2} a_2^\dagger, \tag{27}$$

with

$$c_{N+}^{\iota,j} = \frac{c_+^{\iota,j}}{\lvert c_+^{\iota,1}\rvert^2 + \lvert c_+^{\iota,2}\rvert^2} \tag{28}$$

The relation (27) defines a canonical transformation satisfying

$$[\mathcal{A}_\iota, \mathcal{A}_\iota^\dagger] = 1; \qquad \lvert c_{N+}^{\iota,1}\rvert^2 + \lvert c_{N+}^{\iota,2}\rvert^2 = 1. \tag{29}$$

This transformation may be a good approximation as long as the contributions $|c_-^{\iota,j}|$ are small compared with $|c_+^{\iota,j}|$. This is indeed the situation for an ideal molecule with local mode behavior. For carbon dioxide, this is not the case, but we propose to apply the canonical transformation (27) to obtain a local representation without breaking the polyad and providing the possibility of mapping the local bosonic operators to ladder operators associated with Morse functions. Here it is convenient to clarify the use of polyad in this context. The polyad for the asymmetric isotopologues is the same as for the symmetric isotopologues since the involved interactions in both cases are basically the same. Hence we take into account the set of states (7-9) as part of a polyad even though the state (9) is not really in resonance. However, we retain this name for convenience because it embrace the states of interest. As the contributions of the annihilation operators in the expression (24) could be relevant, we thus define

$$\delta_- = \frac{1}{2}\sum_{\iota=1}^{2}\left[\sum_{j=1}^{2}\lvert c_-^{\iota,j}\rvert^2\right], \tag{30}$$

which measures the feasibility of establishing the canonical transformation (27), but also the degree of locality/normality of a system of equivalent oscillators, as we next show. It is important to clarify that the CO_2 isotopologues have a clear normal mode behaviour, but we are establishing a formal way to measure the degree of this normality, which may also be considered as certain degree of locality. On the other hand, in a previous work [123, 124], it was shown that the parameter γ defined as

$$\gamma = \frac{1}{8}(x_f - x_g)^2; \qquad x_f = \frac{f_{12}}{f_{11}}, \qquad x_g = \frac{g_{12}^{(0)}}{\sqrt{g_{11}^{(0)} g_{22}^{(0)}}}, \tag{31}$$

measures the locality degree, in such a way that in the exact local limit $\gamma = 0$. Therefore, the parameters δ_- and γ are independent and both must tend to zero in order to recover the exact local limit. A correlation between the parameters (30) and (31) is then expected. To show this correlation

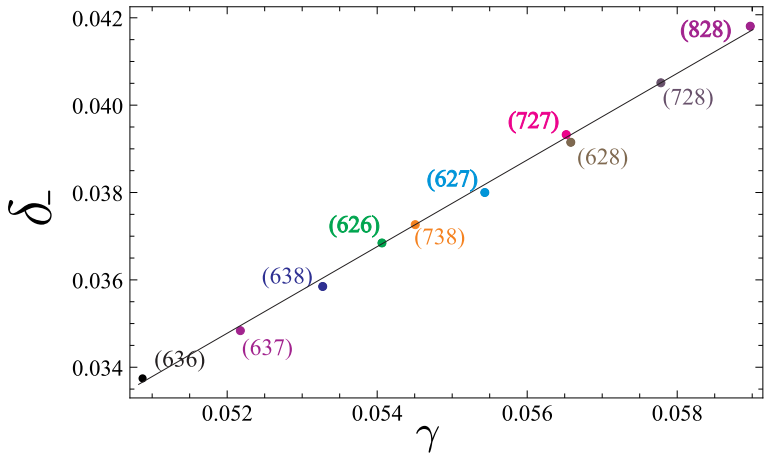

Figure 1: Location of the isotopologues in a diagram δ_- vs γ, where $\gamma = \frac{1}{8}(x_f - x_g)^2$. The force constants used in the calculation of x_f were extracted from the normal scheme. The point for (738) is a prediction.

we present in Figure 1 the plot δ_- vs γ. It is clear that this plot allows the quantitative measure of the degree of locality/normality, using only the fundamentals of the molecule.

We should stress that the linear behavior with slope m in Figure 1 establishes the equation

$$\delta_- = m\ \gamma + b, \tag{32}$$

satisfied for any isotopologue. The linear fit shown in Figure 1 provides the values $m = 0.998248$ and $b = -0.0171966$. In addition, in the same works [123, 124], in order to measure the degree of locality (normality) for the case of two equivalent oscillators, the parameter ζ was introduced

$$\zeta = \left| \frac{2}{\pi} \arctan\left(\frac{(E_1 - E_2)}{(E_1 + E_2)/2} \right) \right|, \tag{33}$$

which is based on the fact that the splitting of the fundamentals are expected to be small in the local limit. In Figure 2 the plot ζ vs γ is displayed. We see an almost linear trend in the distribution of all the isotopologues, which manifests the degree of locality. It is clear that in both figures the isotopologue (636) is located at the extreme of locality due to the heavier central atom, while the isotopologue (828) presents the extreme normality due to the heavier ending atoms. In both figures the symmetric isotopologues were included using the results given in the Appendix C. Again the linear trend establishes the relation

$$\zeta = m'\gamma + b', \tag{34}$$

with $m' = 2.25042$ and $b' = 0.215731$, which may be useful to determine the missing fundamental frequency not available from experiment for a given isotopologue. For example, for the isotopologue (738) we have $\gamma = 0.054567$ with the identified fundamental $\omega_3 = 2255.95$ cm^{-1}. Using the expression (34) we obtain $\omega_1 = 1230.34$, not identified experimentally. This value may be used as the initial guess to obtain the complete rovibrational description. It is clear, however, that the best approach to estimate the fundamental is through the potential surface energy obtained from the other isotopologues. Based on this analysis we now proceed to establish the model to describe the vibrational excitations.

It is also interesting to exhibit in Fig. 3 the correlation between the strength of the Fermi interaction and the local-to-normal mode behavior at this level of approximation. Although a uniform linear trend is not manifested, the correlation of the strength of the Fermi interaction with the local/normal character is still present.

3 Vibrational description

We found that for the asymmetric isotopologues a good option to estimate the force constants is to use the normal mode scheme. To accomplish this plan we may follow the same procedure followed

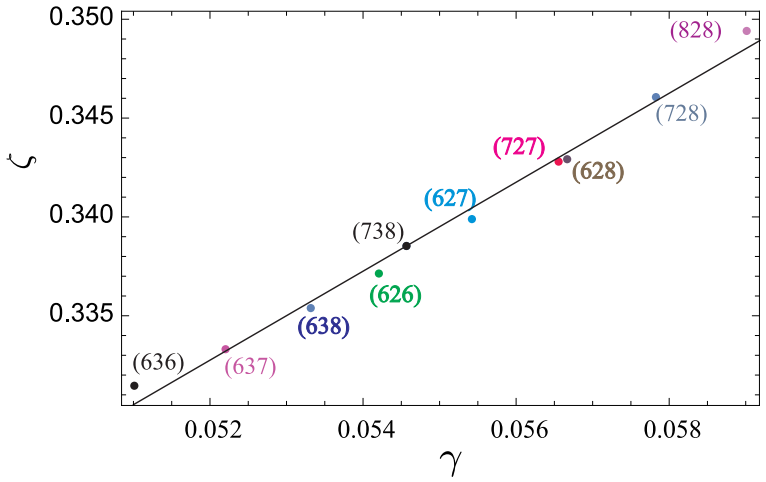

Figure 2: Location of the isotopologues in a diagram ζ vs γ, where $\zeta = |\frac{2}{\pi}\arctan(E_1 - E2)/\bar{E}|$ and $\gamma = \frac{1}{8}(x_f - x_g)^2$ with $\bar{E} = (E_1 + E_1)/2$. The force constants used in the calculation of x_f were extracted from the normal scheme. The point for (738) is a prediction.

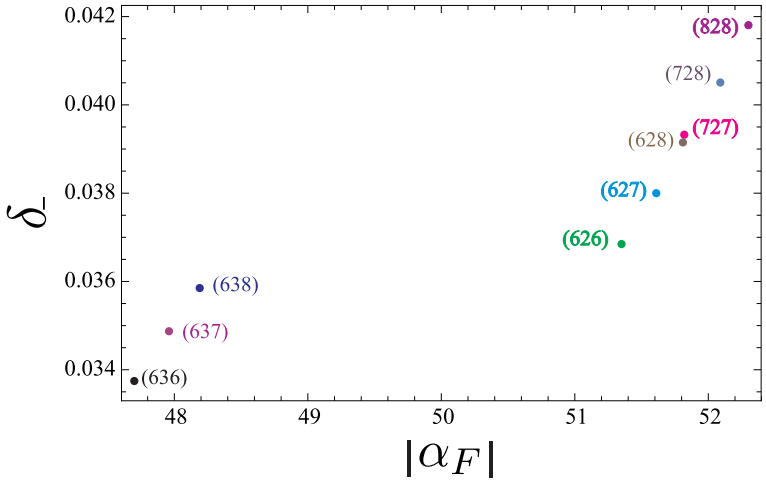

Figure 3: Location of the isotopologues in a diagram δ_- vs α_F, taking the values displayed in Table 3.

in the previous analysis where we started from configuration space in terms of normal coordinates to get an algebraic Hamiltonian. This route provides the spectroscopic parameters in terms of the structure and force constants. However, in a general case, given the imposed symmetry over the force constants due to the Born-Oppenheimer approximation, their number turns out to be less than the number of spectroscopic parameters, which means that the higher order force constants cannot be uniquely determined. Instead, we proceed to propose an algebraic expansion from the outset. As a first approximation, the following Hamiltonian is considered where the spectroscopic parameters are fitted taking into account all available experimental energies

$$\hat{H}_0^{(\mathrm{N})} = \sum_{\iota=1,3} \frac{\hbar\Omega_\iota}{2}\left(\mathcal{A}_\iota^\dagger \mathcal{A}_\iota + \mathcal{A}_\iota \mathcal{A}_\iota^\dagger\right) + \frac{\hbar\omega}{2}\sum_{\alpha=+,-}(\tau_\alpha^\dagger\tau_\alpha + \tau_\alpha\tau_\alpha^\dagger) + \sum_{i,j} x_{ij}\hat{\nu}_i\hat{\nu}_j + g_{22}\hat{\ell}^2 + \alpha_F^{(N)}[\mathcal{A}_1^\dagger\tau_+\tau_- + H.c.], \tag{35}$$

where

$$\hat{\nu}_i = \mathcal{A}_i^\dagger \mathcal{A}_i; \qquad i = 1, 3 \tag{36}$$

$$\hat{\nu}_2 = \sum_{\alpha=+,-} (\tau_\alpha^\dagger \tau_\alpha), \tag{37}$$

$$\hat{\ell} = \tau_+^\dagger \tau_+ - \tau_-^\dagger \tau_-, \tag{38}$$

following the standard numbering scheme for the normal modes [81]. This Hamiltonian corresponds to the usual realization in terms of normal modes, justified by the strong normal behaviour of these isotopologues. In this contribution we propose to improve the description by introducing local operators associated with the CO stretching coordinates through the canonical transformation (27) providing a Hamiltonian of the form

$$\hat{H}_0^{(\mathrm{N})} = \hat{H}_0^{(\mathrm{N})}(a_i^\dagger(a_i), \tau_\alpha^\dagger(\tau_\alpha)); \qquad i = 1, 2, \qquad \alpha = +, -. \tag{39}$$

Because of the canonical transformation involved, both Hamiltonians (35) and (39) are equivalent: they provide the same fit to the experimental vibrational energies. However the representation (39) has the advantage that the bosonic local operators $a_i^\dagger(a_i)$ can be mapped to $SU(2)$ operators $b_i^\dagger(b_i)$ associated with ladder operators for the Morse states $|\Psi_v^j\rangle$, while for the bends, the $U(3)$ vibron model can be implemented. Following this route, the vibrational description is improved by taking into account anharmonicities from the outset [127, 128, 129, 130, 131, 132, 133, 134, 135, 136, 137, 138, 139]. In practice, we introduce the following mapping at the local level for the stretching modes

$$a_i^\dagger \to b_i^\dagger, \quad a_i \to b_i \; ; \qquad |v_i\rangle \to |\Psi_{v_i}^j\rangle, \tag{40}$$

with matrix elements

$$\begin{aligned} b_i^\dagger |\Psi_{v_i}^{j_i}\rangle &= \sqrt{(v_i+1)(1-(v_i+1)/\kappa_i)}\; |\Psi_{v_i+1}^{j_i}\rangle \quad , \\ b_i |\Psi_{v_i}^{j_i}\rangle &= \sqrt{v_i(1-v_i/\kappa_i)}\; |\Psi_{v_i-1}^{j_i}\rangle \quad , \\ \hat{v}_i |\Psi_{v_i}^{j_i}\rangle &= v_i |\Psi_{v_i}^{j_i}\rangle, \end{aligned} \tag{41}$$

where v_i is the vibrational quantum number for the i-th oscillator with $v_i = 0, 1, 2, \ldots, j_i - 1$. The parameter $\kappa_i = 2j_i + 1$ is related to the potential depth D, the potential range β and the reduced mass. In the algebraic representation the Morse Hamiltonian takes the form

$$\hat{H}_i^M = \left(b_i^\dagger b_i + b_i b_i^\dagger + \frac{1}{2\kappa_i} \right), \tag{42}$$

with eigenvalues

$$E_M(v_i) = \hbar\omega_i \left[(v_i + 1/2) - \frac{1}{\kappa_i}(v_i + 1/2)^2 \right] \quad , \tag{43}$$

where

$$\omega_i = \sqrt{\frac{2D\beta^2}{\mu_i}}; \qquad \kappa_i = \sqrt{\frac{8D\mu_i}{\hbar^2\beta^2}}. \tag{44}$$

From Eqs. (44) we obtain the relations between the κ''s of the isotopologues:

$$\kappa_i = \sqrt{\frac{g_{jj}^{(0)}}{g_{ii}^{(0)}}}\kappa_j; \quad i, j = 1, 2. \tag{45}$$

Notice that this equation establishes the relations between the κ's and, consequently, the κ for a given isotopologue must be considered as a reference to obtain the parameters κ of the other isotopologues. Our reference will be the principal isotopologue.A similar procedure is carried out for the bends through the $U(3)$ vibron model introducing the mapping

$$\tau_\pm^\dagger \to b_\pm^\dagger, \qquad \tau_\pm \to b_\pm \quad , \tag{46}$$

in the Fermi interaction with matrix elements

$$b_{\pm}^{\dagger}|[N];n^{\ell}\rangle = \sqrt{\left(\frac{n\pm\ell}{2}+1\right)\left(1-\frac{n}{N}\right)}\,|[N];(n+1)^{\ell\pm1}\rangle \quad ,$$
$$b_{\pm}|[N];n^{\ell}\rangle = \sqrt{\left(\frac{n\pm\ell}{2}\right)\left(1-\frac{n-1}{N}\right)}\,|[N];(n-1)^{\ell\mp1}\rangle. \tag{47}$$

In this context, N stands for the total number of bosons (vibrons), which determines the dimension of the available Hilbert space for the bending degree of freedom. These transformations leads to a Hamiltonian of the form

$$\hat{H}_0^{(\mathrm{N})} = \hat{H}_0^{(\mathrm{N})}(N,\kappa_i;\ b_i^{\dagger}(b_i), b_{\alpha}^{\dagger}(b_{\alpha}), \tau_{\alpha}^{\dagger}(\tau_{\alpha})); \qquad i=1,2, \qquad \alpha=+,-, \tag{48}$$

where we have indicated the parametric character of the stretching potential depth κ_i and N for the bends. We have thus started considering the anharmonic version of the potential (35) which takes the form

$$\hat{\mathcal{H}}_0^{(\mathrm{N})} = \hat{H}_0^{(\mathrm{N})}\Big|_{a_i^{\dagger},\tau_{\alpha}^{\dagger}\to b_i^{\dagger},b_{\alpha}^{\dagger}} = \sum_{\iota=1,3}\frac{\hbar\Omega_{\iota}}{2}\left(\mathcal{A}_{\iota}^{\dagger}\mathcal{A}_{\iota}+\mathcal{A}_{\iota}\mathcal{A}_{\iota}^{\dagger}\right)+\frac{\hbar\omega}{2}\sum_{\alpha=+,-}\left(\tau_{\alpha}^{\dagger}\tau_{\alpha}+\tau_{\alpha}\tau_{\alpha}^{\dagger}\right)$$
$$+\sum_{i,j}x_{ij}\{\hat{\nu}_i,\hat{\nu}_j\}+g_{22}\ell^2+\alpha_F^{(\mathrm{N})}\hat{V}_F, \tag{49}$$

with

$$\mathcal{A}_{\iota}^{\dagger} = c_{+}^{\iota,1}b_1^{\dagger}+c_{+}^{\iota,2}b_2^{\dagger}, \tag{50}$$
$$\hat{\nu}_{\iota} = |c_{+}^{\iota,1}|^2 b_1^{\dagger}b_1+|c_{+}^{\iota,2}|^2 b_2^{\dagger}b_2+c_{+}^{\iota,1}c_{+}^{\iota,2}(b_1^{\dagger}b_2+b_1b_2^{\dagger}) \tag{51}$$
$$\hat{\nu}_2 = \sum_{\alpha}\tau_{\alpha}^{\dagger}\tau_{\alpha}, \tag{52}$$
$$\hat{V}_F = [\mathcal{A}_1^{\dagger}b_+b_- + H.c.]. \tag{53}$$

Here we have introduced the notation $\{\hat{A},\hat{B}\}$ for keeping the symmetrization of the operators

$$\{\hat{A},\hat{B}\} = \frac{1}{2}(\hat{A}\hat{B}+\hat{B}\hat{A}), \tag{54}$$

since the number operators stop commuting due to the anharmonization procedure. Here we should notice that the anharmonization for the bends expressed by the matrix elements (47) is involved only in the Fermi interaction. In addition, we also stress that up to now all the interactions conserve any of the polyads considered to describe the CO_2, since we have chosen an expansion in terms of normal modes. Although Hamiltonian (49) provides reasonable results, in order to obtain spectroscopic quality with square root deviations of the order of 0.1 cm^{-1}, additional interactions must be included. We have thus found that the Hamiltonian should be extended to

$$\hat{\mathcal{H}}^{(\mathrm{N})} = \hat{\mathcal{H}}_0^{(\mathrm{N})}+\alpha_F^{(1)}\{\hat{\nu}_1,\hat{V}_F\}+\alpha_F^{(3)}\{\hat{\nu}_3,\hat{V}_F\}+d_N\hat{D}, \tag{55}$$

where $\hat{D}$ is the Darling-Dennison interaction given by

$$\hat{D} = \mathcal{A}_1^{\dagger}\mathcal{A}_1^{\dagger}\mathcal{A}_3\mathcal{A}_3+H.c., \tag{56}$$

which is characteristic of the polyad $P_{212} = 2(\nu_1+\nu_3)+\nu_2$. This polyad has been proved to be convenient after comparing the experimental and the simulated Raman spectra for the three different polyads used for CO_2 [106]. To obtain the parameter κ of local stretching potential we have the relation (45) associated with the individual $^{m_1}\mathrm{C}^{m_2}\mathrm{O}$ bonds. The first guess for the parameter κ can be estimated from the vibrational constants $\omega_e = 2169.82\ \mathrm{cm}^{-1}, \omega_e x_e = -13.293\ \mathrm{cm}^{-1}$, for the $^{12}\mathrm{C}^{16}\mathrm{O}$ molecule [140], since

$$\frac{\omega_e}{\omega_e x_e} \approx 163, \qquad \frac{\omega_e}{\omega_e x_e} = \kappa. \tag{57}$$

This value $\kappa = 163$ can be considered as a starting guess for the principal isotopologue. We have found that the best value to minimize the rms corresponds to $\kappa = 164$. Using the relation (45) we obtain the different κ_i values for the bonds $^{m_1}\mathrm{C}^{m_2}\mathrm{O}$ in accordance with the relation

$$\kappa_i = \sqrt{\frac{(1/12 + 1/16)}{(1/m_1 + 1/m_2)}}\kappa. \tag{58}$$

The results for the different bonds involved in all the series of isotopologues are displayed in Table 6.

Table 6: Values of κ_i using Eq. (58) for the different CO-bonds involved in the different isotopologues. We have taken $\kappa = 164$ corresponding to the principal isotopologue as a reference.

(m_1, m_2)	(12,16)	(12,17)	(12,18)	(13,16)	(13,17)	(13,18)
κ_i	164	166	168	168	170	172

For the $U(3)$ model a potential in the same footing as the SU(2) model is not given. However it was found that the coordinates and momenta are given by [105]

$$\mathcal{Q}_\pm = \frac{1}{\sqrt{2}}\sqrt{\frac{\hbar}{\omega\mu}}(b_\pm^\dagger - b_\mp); \quad \mathcal{P}_\pm = -\frac{i}{\sqrt{2}}\sqrt{\hbar\omega\mu}(b_\mp^\dagger + b_\pm), \tag{59}$$

where the matrix elements of the ladder operators are given in Eq. (47). The quadratic bending Hamiltonian in configuration space is given by

$$\hat{H}_b = -\frac{1}{2}g_{+-}\ (\mathcal{P}_+\mathcal{P}_- + \mathcal{P}_-\mathcal{P}_+) - \frac{1}{2}f_{+-}\ (\mathcal{Q}_+\mathcal{Q}_- + \mathcal{Q}_-\mathcal{Q}_+)\ \ , \tag{60}$$

where the substitution of (59) into the Hamiltonian (60) gives rise to the algebraic representation

$$\hat{H}_b^{\mathrm{alg}} = \hbar\omega\left\{\left(1 - \frac{1}{2N}\right)\hat{n} + 1 - \frac{\hat{n}^2}{N}\right\}, \tag{61}$$

that, when the energies are refered to the ground state, the Hamiltonian can be expressed as

$$\hat{H}_b^{\mathrm{alg}} \approx \hbar\omega\left\{\hat{n} - \frac{\hat{n}^2}{N}\right\}. \tag{62}$$

This expression turns out to be similar to the Morse case (43) and, consequently, we may propose a similar expression to (45)

$$N_i = \sqrt{\frac{g_{aa}^{(0)}(j)}{g_{aa}^{(0)}(i)}}N_j, \tag{63}$$

where i and j correspond to the i-th and j-th isotopologue. Taking again $N_j = N$ as the number of bosons associated with the principal isotopologue, we have

$$N_i = \sqrt{\frac{1/16 + 1/16 + 4/12}{1/m_{O_1} + 1/m_{O_2} + 4/m_C}}N. \tag{64}$$

Eq.(62) provides a way to estimate N for the principal isotopologue by taking the energies for the states (01^10) and (03^10) corresponding to $E_1 = 667.38$ cm^{-1} and $E_2 = 1932.47$ cm^{-1}, respectively. The obtained value is $N = 58$, which is taken as a first guess in the fit. The best value turned out to be $N = 154$, from which we obtain the boson numbers displayed in Table 7.

Because of the mappings (40) and (46), this model introduces anharmonicities from the outset, a feature that permits to obtain better fits with a smaller number of parameters, albeit keeping the connection with coordinates and momenta. This means that force constants can be estimated [100].

Table 7: Values of N_i using Eq. (64) for the different isotopologues. We have taken $N = 154$ corresponding to the principal isotopologue as a reference. For convenience we have chosen the closest even number for N. The corresponding values for (κ_1, κ_2) have been included in accordance with Table 6.

Isotopologue	(626)	(636)	(727)	(828)		
N_i	154	158	156	156		
(κ_1, κ_2)	(164,164)	(168,168)	(166,166)	(168,168)		
Isotopologue	(638)	(627)	(628)	(728)	(637)	(738)
N_i	160	154	154	156	160	160
(κ_1, κ_2)	(168,172)	(164,166)	(164,168)	(166,168)	(168,170)	(170,172)

The parameters are optimized by a least square fit to the experimental energies for the given values of κ and N, which are modified for each minimization procedure until the best description is reached. The fits were carried out considering a symmetry adapted basis [141, 142, 143, 144] and all the experimental energies were assigned equal weights. The accuracy of the fit is shown using the usual definition for the root mean square deviation (rms) in terms of the quadratic energy deviation χ^2:

$$\text{rms} = \frac{\chi}{\sqrt{(N_{\text{exp}} - N_{\text{par}})}}; \qquad \chi^2 = \sum_{i=1}^{N_{\text{exp}}} (E^i_{\text{exp}} - E^i_{\text{cal}})^2, \tag{65}$$

where N_{exp} is the total number of fitted experimental energies and N_{par} stands for the number of parameters. During the fit procedure, we distinguish two kinds of parameters. A first set corresponds to the spectroscopic parameters, while a second set are given by the anharmonicities κ and N implicitly involved in the matrix elements. In the fitting procedure κ and N are fixed each time the iterative least square method is applied to optimize the first set of parameters. Following this procedure, by taking different values for the set $\{\kappa, N\}$, we search for the minimum of the root mean square deviation in each fit of the first set of parameters, until we obtain the convergence for the complete set of parameters. To determine the significance of the fits, a statistical error analysis was carried out. Two types of uncertainty calculations are given for all the parameters (x_i): the delta-uncertainty (δx_i) and the epsilon-uncertainty (ϵx_i) [145, 146]. They are defined in such a way that χ^2 does not increase more than a fraction Δ (in all fits the value was taken to be Δ=0.05) of the minimum value χ^2_{min}. The uncertainty δx_i is defined through the condition that χ^2 remains under $(1 + \Delta)$ χ^2 when x_i is chosen in the interval $[x_i - \delta x_i, x_i + \delta x_i]$ around its optimum value x_i, keeping fixed the rest of the parameters. On the other hand, ϵx_i determines the range in which x_i varies when all other parameters are optimized again.

3.1 Results for the vibrational energies of the CO_2 isotopologues

We now start presenting the results for the series of the studied isotopologues in the framework of the polyad $P_{212} = 2(\nu_1 + \nu_3) + \nu_2$, which has been proved as the best option for the simulation of the Raman spectra. In our vibrational study, updated experimental energy levels were considered in the fit.

Isotopologue (638)

For the isotopologue $^{16}O^{13}C^{18}O$ (638), 40 energies up to 9,300 cm^{-1} including polyad $P_{212} = 11$ have been reported. First we have considered the Hamiltonian (49) involving 11 parameters, which provided a fit with an rms=0.76 cm^{-1}. This vibrational description was considerably improved by adding the interactions $\{\hat{\nu}_1, \hat{V}_F\}$ and $\{\hat{\nu}_3, \hat{V}_F\}$, which introduce the coupling of the Fermi resonance with the stretching modes, as well as the Darling-Dennison interaction. The Hamiltonian takes thus

the form (55), which provides the rms=0.0712 cm^{-1} . To evaluate the improvement provided by our model, a fit using the harmonic limit of the Hamiltonian (55) omitting the interactions associated with parameters $\alpha_F^{(1)}, \alpha_F^{(3)}$ and d_N, gives rise to the deviation rms=1.07 cm^{-1}. The addition of the interactions $\alpha_F^{(1)}$ and $\alpha_F^{(3)}$ improves the fit to rms=0.67 cm^{-1}, but Darling-Dennison interaction does not converge.

This analysis was carried out applying the anharmonization procedure (40) for the stretches and (46) for the bends in the Fermi interaction. The effect of the Darling-Dennison interaction is not determinant but it was included because it is the only interaction defining the polyad P_{212}. The optimized parameters are displayed in Table 8, where the uncertainties have been included, showing that they are well determined. In Table S1 of the Supporting Information the fitted energies are displayed. The predicted energies are included in Table S6 of the Supporting Information.

Table 8: Spectroscopy parameters (in cm^{-1}) of the Hamiltonian (55) and their corresponding uncertainties for the isotopologue (638) optimized involving the 40 available experimental vibrational levels. The parameters associated with the potential depth are taken to be $\kappa_1 = 168, \kappa_2 = 172$ and $N = 160$. The criteria of the fit quality χ^2 (in cm^{-2}) and the root mean square deviation rms (in cm^{-1}) are also included.

Parameter	Fit	ϵx_i	δx_i
ω_1	1318.77	0.2119	0.0079
ω_2	643.21	0.0420	0.0037
ω_3	2295.13	0.0431	0.0059
g_{22}	0.3018	0.0511	0.0089
x_{11}	1.0669	0.0324	0.0029
x_{22}	-5.0313	0.0205	0.0025
x_{33}	-0.1467	0.0518	0.0007
x_{12}	3.2816	0.0348	0.0066
x_{13}	1.2832	0.2002	0.0037
x_{23}	-11.7535	0.0146	0.0033
α_F	-48.5166	0.0528	0.0038
$\alpha_F^{(1)}$	0.2899	0.0163	0.0024
$\alpha_F^{(3)}$	0.5171	0.0113	0.0035
d_N	1.0673	0.5755	0.1299
χ^2	0.1319		
rms	0.0712		

Isotopologue (627)

For the isotopologue $^{16}O^{12}C^{17}O$ (627), the number of available experimental energies are 57 embracing polyads up to $P_{212} = 12$ and energies up to 12,800 cm^{-1}. As in the previous isotopologue, we first considered the Hamiltonian (49) involving 11 parameters, which provided a fit with an rms=0.73 cm^{-1}. The addition of the interactions associated with the parameters $\alpha_F^{(1)}$ and $\alpha_F^{(3)}$ in the Hamiltonian (55) reduces the root means square deviation to rms=0.10 cm^{-1}. Finally we included the Darling-Dennison interaction to obtain an rms=0.099 cm^{-1}. The optimized parameters are displayed in Table 9, where the uncertainties have also been included, showing a good convergence. In Table S2 and S7 of the Supporting Information the fitted and the predicted energies are displayed, respectively.

Table 9: Spectroscopic parameters (in cm^{-1}) of the Hamiltonian (55) together with the corresponding uncertainties for the isotopologue (627) using the Hamiltonian (55) optimized involving the 57 available experimental vibrational levels. The parameters associated with the potential depth are taken to be $\kappa_1 = 164, \kappa_2 = 166$ and $N = 154$. The criteria of the fit quality χ^2 (in cm^{-2}) and the root mean square deviation rms in cm^{-1}) are also included.

Parameter	Fit	ϵx_i	δx_i
ω_1	1335.88	0.3636	0.0129
ω_2	664.64	0.0555	0.0056
ω_3	2371.21	0.0534	0.0086
g_{22}	-0.2274	0.0824	0.0081
x_{11}	1.1315	0.0427	0.0051
x_{22}	-5.5237	0.0271	0.0003
x_{33}	0.3876	0.0782	0.0012
x_{12}	3.6905	0.0439	0.0122
x_{13}	-0.7651	0.3228	0.0078
x_{23}	-12.6533	0.0211	0.0051
α_F	-52.0349	0.0439	0.0064
$\alpha_F^{(1)}$	0.4805	0.0338	0.0049
$\alpha_F^{(3)}$	0.4029	0.0226	0.0057
d_N	0.8613	0.9261	0.1308
χ^2	0.43		
rms	0.10		

Isotopologue (628)

The isotopologue $^{16}O^{12}C^{18}O$ (628) presents 95 reported experimental energy terms up to polyad $P_{212} = 20$ with energies up to $22,200$ cm^{-1}. A first fit with 11 parameters provided an rms=0.87 cm^{-1}, which was reduced using the Hamiltonian (55) to an rms=0.43 cm^{-1}. Since the quality of this description is somewhat far from the previous cases, in order to reach the same level of accuracy, we decided to include the next order in the anharmonicities given by

$$\hat{V} = \sum_{i=1}^{3} y_{iii}\ \hat{\nu}_i^3 + \sum_{i\neq j} y_{iij}\ \{\hat{\nu}_i^2, \hat{\nu}_j\} + y_{123}\ \nu_2\{\hat{\nu}_1, \hat{\nu}_3\}, \tag{66}$$

This Hamiltonian, including 23 parameters, provided a fit with an rms=0.22 cm^{-1}. Although this description can be considered of a good quality, it is still far from the results obtained for the other cases considering the increase of the number of parameters. Hence we have decided to suppress the set of experimental energies leading to such large deviation. Using the Hamiltonian (55) with 13 parameters and considering only 90 of the available experimental energies up to 13,600 cm^{-1}, polyad $P_{212} = 12$, we obtained $\chi^2 = 2.34$ cm^{-2} and a deviation of rms=0.17 cm^{-1}. This description is indeed of the expected spectroscopic quality. The five experimental energies taken out from the fit belong to the symmetry Σ^+ and to the polyads 14, 16, 18 and 20 with energies up to 22,200 cm^{-1}. Their predictions obtained from Hamiltonian (55) are given in Table 10. When the states $(0, 0, 7)$ and $(5, 4, 0)$, both of the same polyad 14, are included in the fit, the deviation raised to $\chi^2 = 8.75$ cm^{-2} with rms=0.33 cm^{-1}. This increase may be considered not significant, and including the whole set of 5 energies we have $\chi^2 = 15.4$ cm^{-2} with rms=0.43 cm^{-1}. This increase is unexpected given the predictions associated with the lower polyads in the fitting process. We have thus decided to consider the fit with the 90 energies. The optimized parameters are displayed in Table 11. The fit involving 90 energies are presented in Table S3 of the Supporting Information. The predicted energies obtained from this fit are given in Table S8 of the Supporting Information.

Table 10: Predictions for the isotopologue (628) provided by the fit of the 90 experimental energies using the Hamiltonian (55) with 13 parameters.

Polyad	Normal label	Coefficient	Exp. energy	Theor. energy	Residual
14	$1_5 2_4$	0.2880	9412.75[28]	9409.03	3.7
14	3_7	0.9999	15806.6[157]	15808.0	-1.4
16	3_8	0.9999	17966.7[157]	17969.4	-2.7
18	3_9	0.9999	20102.2[157]	20107.2	-5.0
20	3_{10}	0.9999	22213.4[157]	22221.5	-8.1

Table 11: Spectroscopic parameters (in cm^{-1}) of the Hamiltonian (55) together with their corresponding uncertainties for the isotopologue (628) optimized involving 90 of the 95 available experimental vibrational levels. The parameters associated with the potential depth are taken to be $\kappa_1 = 164, \kappa_2 = 168$ and $N = 154$. The criteria of the fit quality χ^2 (in cm^{-2}) and the root mean square deviation rms (in cm^{-1}) are also included.

Parameter	Fit	ϵx_i	δx_i
ω_1	1318.13	0.0831	0.0079
ω_2	662.23	0.0409	0.0037
ω_3	2363.09	0.0335	0.0069
g_{22}	-0.0350	0.0264	0.0091
x_{11}	1.1282	0.0157	0.0022
x_{22}	-5.5298	0.0090	0.0018
x_{33}	0.2055	0.0045	0.0007
x_{12}	3.6449	0.0280	0.0097
x_{13}	-	-	-
x_{23}	-12.5604	0.0142	0.0043
α_F	-52.3159	0.0162	0.0043
$\alpha_F^{(1)}$	0.4312	0.0076	0.0025
$\alpha_F^{(3)}$	0.4571	0.0080	0.0052
d_N	1.0067	0.3199	0.1163
χ^2	2.34		
rms	0.17		

Isotopologue (728)

For the isotopologue $^{17}O^{12}C^{18}O$ (728), the number of available experimental energies are 42, embracing polyads up to $P_{212} = 10$ and energies up to 7,780 cm^{-1}. Here we consider the Hamiltonian (55) with 14 parameters giving rise to a root means square deviation of rms=0.058 cm^{-1}. The optimized parameters are displayed in Table 12, where the uncertainties have been included, showing a good convergence. In Table S4 of the Supporting Information the fitted energies are displayed. The predicted energies are included in Table S9 of the Supporting Information.

Isotopologue (637)

For the isotopologue $^{16}O^{13}C^{17}O$ (637), the number of available experimental energies are 28, embracing polyads up to $P_{212} = 10$ and energies up to 7,700 cm^{-1}. In this case we considered 13 parameters of the Hamiltonian (55), giving rise to a root mean square deviation of 0.058 cm^{-1}. The optimized parameters are displayed in Table 13, where the uncertainties have been included. With the exception of the parameter g_{22}, we have a good convergence consequence of the lack of experimental energies involving several projections of the angular momentum. In Table S5 and S10 of the Supporting Information the fitted and predicted energies are given, respectively.

Isotopologue (738)

For the isotopologue $^{17}O^{13}C^{18}O$ (738), the number of available experimental energies are 12, up to polyad $P_{212} = 8$ and energies up to 7,870 cm^{-1}. Here we face the problem that the frequencies in resonance with the Fermi interaction for $P_{212} = 2$ are not experimentally available. In order to reduce this problem we have invoked the linear relation (34) to obtain the estimation of the frequency $\omega_1 = 1230.34$ cm^{-1}. On the other hand, the initial guess for the Fermi interaction is obtained using an average of the estimation of the force constants displayed in Table 4. We then proceed with a first fit to 13 energies (the 12 experimental ones plus the estimated term value for the fundamental ν_1), optimizing the parameters up to quartic order (excluding Darling-Dennison interaction) to obtain an rms=0.38 cm^{-1}. The optimized parameters are displayed in Table 14, where the uncertainties have

Table 12: Spectroscopy parameters (in cm^{-1}) of the Hamiltonian (55) and the corresponding uncertainties for the isotopologue (728) optimized involving the 42 available experimental vibrational levels. The parameters associated with the potential depth are taken to be $\kappa_1 = 166, \kappa_2 = 168$ and $N = 156$. The criteria of the fit quality χ^2 (in cm^{-2}) and the root mean square deviation (in cm^{-1}) are also included.

Parameter	Fit	ϵx_i	δx_i
ω_1	1296.82	0.1164	0.0048
ω_2	659.58	0.0289	0.0023
ω_3	2352.90	0.0218	0.0039
g_{22}	-0.3023	0.0283	0.0069
x_{11}	1.2120	0.0149	0.0019
x_{22}	-5.47215	0.0078	0.0018
x_{33}	0.4695	0.0182	0.0005
x_{12}	3.7752	0.0200	0.0045
x_{13}	-0.9918	0.0839	0.0032
x_{23}	-12.4631	0.0138	0.0020
α_F	-52.0669	0.0412	0.0026
$\alpha_F^{(1)}$	0.5405	0.0079	0.0019
$\alpha_F^{(3)}$	0.3524	0.0091	0.0023
d_N	-0.0204	0.0106	0.0015
χ^2	0.11		
rms	0.06		

Table 13: Spectroscopy parameters (in cm^{-1}) of the Hamiltonian (55) and the corresponding uncertainties for the isotopologue (637) optimized involving the 28 available experimental vibrational levels. The parameters associated with the potential depth are taken to be $\kappa_1 = 168, \kappa_2 = 170$ and $N = 160$. The criteria of the fit quality χ^2 (in cm^{-2}) and the root mean square deviation (in cm^{-1}) are also included.

Parameter	Fit	ϵx_i	δx_i
ω_1	1336.30	0.0799	0.0061
ω_2	645.64	0.0334	0.0031
ω_3	2303.45	0.0378	0.0047
g_{22}	-0.0081	0.0135	0.0059
x_{11}	1.0355	0.0245	0.0022
x_{22}	-5.0041	0.0211	0.0020
x_{33}	0.1517	0.0048	0.0006
x_{12}	3.2143	0.0649	0.0058
x_{13}	-	-	-
x_{23}	-11.7978	0.0155	0.0029
α_F	-48.5142	0.02005	0.0033
$\alpha_F^{(1)}$	0.3572	0.0090	0.0023
$\alpha_F^{(3)}$	0.4085	0.0155	0.0031
d_N	2.4693	1.2211	0.1601
χ^2	0.05		
rms	0.06		

been included, showing a good convergence. Although this fit present a small rms, we have too many parameters compared with the number of energies. In addition we notice the value $x_{12} = 16.69$ cm^{-1}, is clearly far from the average $x_{12} \approx 3.0$ cm^{-1} for the other isotopologues. Another point is that there is only one energy belonging to symmetry Π and, consequently, it is not enough to stabilize the parameter g_{22}. Hence, in this case, an strategy must be proposed to obtain a confident fit that provide reasonable wave functions. To achieve this goal we have analyzed simultaneously the wave functions

together with the fit of energies, a task that will be done in the next subsection.

Table 14: Spectroscopy parameters (in cm^{-1}) of the Hamiltonian (55) with the corresponding uncertainties for the isotopologue (738) optimized involving $12+1$ experimental vibrational levels. The parameters associated with the potential depth are taken to be $\kappa_1 = 170, \kappa_2 = 172$ and $N = 160$. The criteria of the fit quality χ^2 (in cm^{-2}) and the root mean square deviation (in cm^{-1}) are also included.

Parameter	Fit 1	ϵx_i	δx_i
ω_1	1289.8	0.2242	0.0103
ω_2	643.01	0.1011	0.0052
ω_3	2283.09	0.0508	0.0068
g_{22}	-1.8610	0.1158	0.0350
x_{11}	0.5629	0.0498	0.0045
x_{22}	-4.4222	0.0182	0.0027
x_{33}	-0.5841	0.0348	0.0012
x_{12}	16.6918	0.1421	0.0106
x_{13}	3.2467	0.1672	0.0105
x_{23}	-14.3516	0.0442	0.0045
α_F	-47.9495	0.02327	0.0059
χ^2	0.29		
rms	0.38		

3.2 Wave functions

The fits for the different isotopologues provide wave functions useful to simulate the Raman spectra. In particular the four transitions given in Table 15 give rise to the most intense lines in the spectra. Given the correlation between δ_- and γ displayed in Figure 1, we wonder about a possible correlation between the two components $\{a, a'\}$ and the degree of locality. In Table 16 a summary of the relevant results is presented, while in Figure 4 we display the plot of the components of the wave functions for both symmetries versus δ_-. With the exception of the isotopologue (738), it is clear the correlation between the locality degree and the components. This fact suggests a similar correlation for the relative strength of the corresponding lines in the Raman spectra. Let us now consider the isotopologue (738), characterized by the suspicious values of x_{12} and g_{22} in the fit provided by Table 14. The corresponding states components provided by this fit have been pointed out as "Fit 1" in Figure 4. Since the components are quite different from the general trend for the rest of the isotopologues, we conclude that the corresponding wave functions lack of physical sense. Hence we have decided to look for a fit where the components of the wave functions are close to the straight line. This can be accomplish by identifying the parameters that have an effect over the components of the wave functions, which turn out to be precisely g_{22} and x_{12}. First the latter parameter was fixed to $x_{12} = 3.5214$ cm^{-1} in accordance to the average the other isotopologues. In addition, since the g_{22} parameter is expected to be close to $g_{22} = \pm 0.3$ cm^{-1} according to the fits for the other isotopologues, we proceeded to carry out a new fit starting with a frozen parameter $g_{22} = -0.3$ cm^{-1}. In the next steps, the parameters g_{22} and x_{12} were modified manually to obtain the best fit taking care that the wave functions agree with the linear trend. The result is given in Table 17. The components of the wave functions were also included in Figure 4 with label "Fit 2". Although this fit is not as good as the others, it keeps the physical meaning according to the wave functions.

The analysis of the components a,a' *vs* δ_- has been also carried out for the symmetric isotopologues using the results given in the Appendix. In Figure 5 the results for all the isotopologues are displayed. In these diagrams we have supposed a linear trend, just to emphasize the correlation between the components of the wave functions and the normal/local character. However we are aware that this relation may not follow the linear behavior for some of the isotopologues.

Finally, it is convenient to show the change of the strength of the Fermi interaction when the global fit is carried. In Table 18 the results from Tables 3 and 19 as well as from the global fits are displayed. We can see that the Fermi interaction is pretty stable, showing the general trend with respect to

Table 15: Wave functions and transition energies involved in the most intense lines in theRaman spectrum obtained in this work from the fits for the different isotopologues . Given the normalization, the parameters a and a' determines the transition strength. The transition energies were taken from experimental results.

Symmetry	(637)	(638)	(627)	(628)	(728)	$\|\nu\rangle \rightarrow \|\nu'\rangle$
Σ^+	1255.33	1244.90	1272.35	1259.42	1244.59	$\|00^00\rangle \rightarrow a\|10^00\rangle + b\|02^00\rangle$
Σ^+	1355.12	1342.27	1376.13	1365.84	1355.74	$\|00^00\rangle \rightarrow b\|10^00\rangle - a\|02^00\rangle$
$\Pi^\pm$	1236.84	1225.91	1251.92	1239.35	1224.94	$\|01^{\pm1}0\rangle \rightarrow a'\|11^{\pm1}0\rangle + b'\|03^{\pm1}0\rangle$
$\Pi^\pm$	1374.41	1362.11	1397.38	1386.95	1376.32	$\|01^{\pm1}0\rangle \rightarrow b'\|11^{\pm1}0\rangle - a'\|03^{\pm1}0\rangle$

Table 16: Summary of the fits for the complete series of asymmetric isotopologues. The components of the wave functions as well as the parameter δ_- are also included.

Isotopologue	(637)	(638)	(738)*	(627)	(628)	(728)
No. Energies	28	40	13	57	90	42
No. Parameters	12	14	10	14	14	13
rms	0.056	0.068	0.26	0.10	0.15	0.065
a	0.604859	0.645312	0.747715	0.75071	0.794356	0.830245
a'	0.636241	0.656285	0.722074	0.743765	0.778424	0.805748
δ_-	0.03487	0.03594	0.03717	0.038035	0.03915	0.04051

the local/normal transition. The next work will be to look for a correlation between the degree of normality and the Raman intensities.

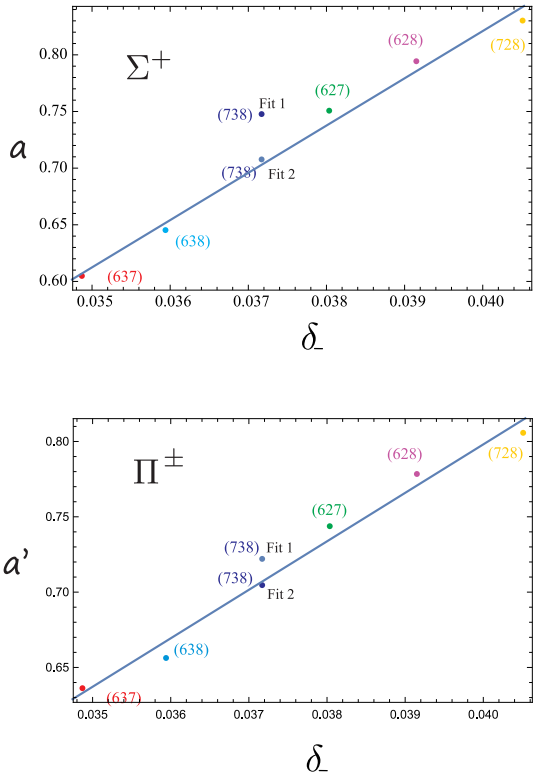

Figure 4: Components of the wave function for the Σ^+ states (a) and $\Pi^\pm$ (a') states with respect to the parameter δ_- defined in Eq. (30). Two points for isotopologue (738) marked by Fit 1 and Fit 2 are given (for more details, see the text).

Table 17: Spectroscopy parameters (in cm^{-1}) and the corresponding uncertainties for the isotopologue (738) optimized to 12+1 energies using 8 free parameters plus two frozen parameters (g_{22} and x_{12}) of the Hamiltonian (55). The parameters g_{22} and x_{12} were optimized manually to obtain good wave functions. The criteria of the fit quality χ^2 (in cm^{-2}) and the root mean square deviation (in cm^{-1}) are also included.

Parameter	Fit 2	ϵx_i	δx_i
ω_1	1295.69	0.5034	0.01482
ω_2	639.81	0.1510	0.0251
ω_3	2285.07	0.1826	0.0323
g_{22}	0.3	-	-
x_{11}	1.8387	0.1486	0.0213
x_{22}	-5.1794	0.0637	0.0130
x_{12}	3.5214	-	-
x_{13}	1.0963	0.1445	0.0473
x_{23}	-10.8184	0.0820	0.0235
α_F	-48.3130	0.0354	0.0275
χ^2	6.51		
rms	1.14		

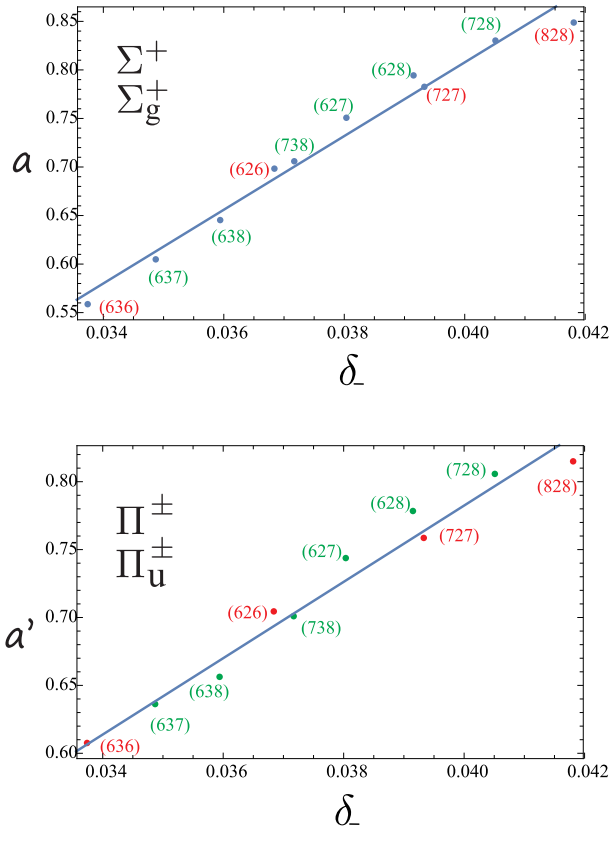

Figure 5: Components of the wave function for the $\Sigma^+(\Sigma_g^+)$ states (a) and $\Pi^\pm(\Pi_u^\pm)$ (a') states with respect to the parameter δ_- defined in Eq. (30) for all the isotopologues, symmetric and asymmetric.

Table 18: Comparison of the strength of the Fermi interactions obtained from the normal mode approximation $\alpha_F^{(N)}$ in Eq. (20) and from the global fits $\alpha_F^{(G)}$ taking into account all the interactions needed to obtain fits of spectroscopic quality.

Isotopologue	$\alpha_F^{(N)}$	$\alpha_F^{(G)}$
(828)	-52.30	-52.89
(728)	-52.09	-52.01
(727)	-51.82	-52.54
(628)	-51.81	-51.92
(627)	-51.61	-52.03
(626)	-51.35	-51.97
(638)	-48.19	-48.45
(637)	-47.96	-48.54
(636)	-47.70	-48.73

4 Summary and conclusions

In this contribution we have extended our study of symmetric isotopologues of carbon dioxide ($^{13}C^{16}O_2$, $^{12}C^{18}O_2$ and $^{12}C^{17}O_2$) to the asymmetric isotopologues $^{16}O^{12}C^{18}O$, $^{16}O^{12}C^{17}O$, $^{16}O^{13}C^{18}O$, $^{16}O^{13}C^{17}O$, $^{17}O^{13}C^{18}O$ and $^{17}O^{12}C^{18}O$. Based on our previous work on the principal isotopologue we have developed our study in the framework of a polyad-conserving Hamiltonian associated with polyad P_{212}. We started our analysis by searching the appropriate selection of coordinates to describe the asymmetric isotopologues. We found convenient to express the normal modes in terms of the symmetry adapted basis to identify the stretching Σ^+ mode involved in the Fermi resonance. In order to show the importance of this coordinate selection, the force constants were estimated first considering a scheme in terms of symmetry adapted coordinates and, later on, in terms of normal modes. Both approaches provided similar results. A crucial analysis was based on the Bogoliubov transformation between the bosonic normal operators and the local bosonic operators. This allowed the introduction of the parameter δ_-, which in the same way as the parameters γ and ζ, establishes a criterion to measure the degree of normality/locality. These parameters are independent but shows a linear correlation for the whole series of isotopologues, including the symmetric ones. We stress that the analysis of the local/normal degree proposed in this work is general and can be applied to any set of equivalent oscillators. This is in contrast to the traditional approach where the study of the local to normal transition was constrained to molecules presenting a strong local behavior, like the ones involving X-H bonds. The criteria presented here allows the possibility to study the local-to-normal mode transition including any molecular system.

In addition to the study of the local-to-normal mode analysis, an algebraic approach was applied to describe the vibrational excitations of the asymmetric isotopologues. Since the CO_2 isotopologues present a strong normal mode behavior, a local mode model cannot be proposed from the outset. Starting with a model in terms of bosonic normal operators, a polyad-conserving canonical transformation in terms of local operators was applied, which were mapped to SU(2)-Morse ladder operators. A similar mapping was applied for the bends in the framework of the $SU(3)$ model.

An exhaustive search of experimental energy levels for all the isotopologues was carried out. The isotopologues $^{16}O^{13}C^{18}O$ (638), $^{17}O^{12}C^{18}O$ (728) and $^{16}O^{12}C^{17}O$ (627), involving 40, 42 and 57 experimental energies, were well described with deviations rms=0.071 cm^{-1}, rms=0.058 cm^{-1} and rms=0.099 cm^{-1}, respectively. Regarding the isotopologue $^{16}O^{12}C^{18}O$ (628), a total of 95 experimental energies are available. In this case the fit including 11 parameters provided an rms=0.43 cm^{-1}. Since the quality of this fit was not as good as for the previous isotopologues we explored the description adding 9 interactions corresponding to the cubic anharmonicities. The rms reduced to 0.22 cm^{-1}. Since this accuracy was not of the quality we expected, given the number of parameters, we decided to consider the subset of 90 experimental energies up to polyad P_{212}=12 using the Hamiltonian (55) with 14 parameters, providing a deviation rms=0.15 cm^{-1}, which is of the same level of accuracy for the previous cases. The isotopologue $^{16}O^{13}C^{17}O$ (637), presents only 28 experimental energies, and with 13 parameters we obtained a root means square deviation of rms=0.054 cm^{-1}. Finally, for the isotopologue $^{17}O^{13}C^{18}O$ (738), just 12 experimental energies are available, but the stretching fundamental band that determines the Fermi interaction is not yet observed. Consequently we took advantage of the BO approximation through the linear trend ζ *vs* γ to estimate the missing fundamental. In addition, we took advantage of the connection between the parameter δ_- and the components of the wave functions to obtain reasonable wave functions.

The vibrational description taking the polyad P_{212} for all the studied isotopologues can be considered of spectroscopic quality. Because of this polyad-conserving restriction, the space of the wave functions is limited, but a previous study proved the advantage of considering this polyad scheme to deal with the simulation of the Raman spectra. We have also included the analysis of the wave functions involved in the strongest intensity lines of the Raman spectrum. We have found that the degree of normality is proportional to the amplitude of the components of the wave functions, a fact that may be useful in the identification of the Raman spectra involving a mixture of isotopologues. This conclusion is possible due to the incorporation in our study of the symmetric isotopologues previously considered.

5 Supporting information

The fits and predictions of the vibrational energies of the asymmetric isotopologues (638), (627), (628), (728), and (637) are given as supporting information.

6 Acknowledgments

This work is partially supported by DGAPA-UNAM, Mexico, under project IN-212020. M.C. acknowledges the financial support from the European Union's Horizon 2020 research and innovation program under the Marie Skłodowska-Curie grant agreement No 872081 and from grant PID2019-104002GB-C21 funded by MCIN/AEI/10.13039/501100011033 and, as appropriate, by 'ERDF A way of making Europe', by the 'European Union' or by the 'European Union NextGenerationEU/PRTR'. This work has also been partially supported by the Consejería de Transformación Económica, Industria, Conocimiento y Universidades, Junta de Andalucía and European Regional Development Fund (ERDF 2014-2020) PY2000764.

Appendix A. Coordinates transformation to obtain the algebraic Hamiltonian

In order to obtain an algebraic representation of the Hamiltonian (1) we first introduce the polar coordinates for the bends

$$Q_+ = -\frac{1}{\sqrt{2}}(q_a + iq_b); \qquad Q_- = \frac{1}{\sqrt{2}}(q_a - iq_b), \tag{67}$$

with associated momenta $\{P_+, P_-\}$ and the symmetrized linearized internal coordinates(corresponding to the normal coordinates for the symmetric isotopologues)

$$S_g = \frac{1}{\sqrt{2}}(q_1 + q_2); \qquad S_u = \frac{1}{\sqrt{2}}(q_1 - q_2), \tag{68}$$

with the conjugate momenta $\{\Pi_g, \Pi_u\}$. We may substitute (67) and (68) into (1) to obtain the Hamiltonian in these new coordinates and, so, to introduce the algebraic realization of the bending coordinates in terms of the bosonic ladder operators $\tau_\pm^\dagger(\tau_\pm)$:

$$Q_+ = \frac{1}{\sqrt{2}}\sqrt{\frac{\hbar}{\omega\mu}}(\tau_+^\dagger - \tau_-); \qquad Q_- = \frac{1}{\sqrt{2}}\sqrt{\frac{\hbar}{\omega\mu}}(\tau_-^\dagger - \tau_+), \tag{69}$$

$$P_+ = -\frac{i}{\sqrt{2}}\sqrt{\hbar\omega\mu}(\tau_-^\dagger + \tau_+); \qquad P_- = -\frac{i}{\sqrt{2}}\sqrt{\hbar\omega\mu}(\tau_+^\dagger + \tau_-), \tag{70}$$

where $\omega = \sqrt{g_{aa}^{(0)} f_{aa}}$ and $\mu = 1/g_{aa}^{(0)}$. In a similar form for the coordinates (68) and the corresponding momenta, the symmetrized coordinates are expressed in terms of the ladder operators $a_g^\dagger$ (a_g) and $a_u^\dagger$ (a_u):

$$S_g = \frac{1}{\sqrt{2}}\sqrt{\frac{\hbar}{w_g\mu_g}}(a_g^\dagger + a_g); \qquad S_u = \frac{1}{\sqrt{2}}\sqrt{\frac{\hbar}{w_u\mu_u}}(a_u^\dagger + a_u), \tag{71}$$

$$\Pi_g = \frac{i}{\sqrt{2}}\sqrt{\hbar w_g\mu_g}(a_g^\dagger - a_g); \qquad \Pi_u = \frac{i}{\sqrt{2}}\sqrt{\hbar w_u\mu_u}(a_u^\dagger - a_u), \tag{72}$$

where $\omega_g = \sqrt{F_{gg}G_{gg}^{(0)}}$, and $\omega_u = \sqrt{F_{uu}G_{uu}^{(0)}}$, with $\mu_g = 1/G_{gg}^{(0)}$ and $\mu_u = 1/G_{uu}^{(0)}$. The Wilson matrix elements and the force constants of the symmetrized coordinates written in terms of the local components are:

$$G_{gg}^{(0)} = \frac{1}{2}(g_{11}^{(0)} + g_{22}^{(0)} + 2g_{12}^{(0)}); \qquad G_{uu}^{(0)} = \frac{1}{2}(g_{11}^{(0)} + g_{22}^{(0)} - 2g_{12}^{(0)}) \ , \tag{73}$$

$$F_{gg} = (f_{11} + f_{12}); \qquad F_{uu} = (f_{11} - f_{12}) \ , \tag{74}$$

where we have taken into account that $f_{11} = f_{22}$ given the Born-Oppenheimer approximation. In addition, it is convenient to introduce the following definitions and relations for the derivatives of the Wilson matrix

$$\left(\frac{\partial g_{2a}}{\partial q_a}\right)_0 = \left(\frac{\partial g_{1a}}{\partial q_a}\right)_0, \tag{75}$$

$$\left(\frac{\partial g_{aa}}{\partial q_2}\right)_0 = \left(\frac{\partial g_{aa}}{\partial q_1}\right)_0 + \gamma; \qquad \gamma = \frac{2}{r_e}(1/m_{O_1} - 1/m_{O_2}), \tag{76}$$

for equilibrium distances $r_{e1} = r_{e2} = r_e$.m_{O_i} stands for the masses of the isotopes of oxygen.

Appendix B. Limit of the approach for the symmetric isotopologues

Here we take advantage of the analysis of Section 2 to present the case of symmetric isotopologues represented by the limit $g_{22}^{(0)} \to g_{11}^{(0)}$. In this case the symmetry adapted coordinates coincide with the normal coordinates and, consequently, the corresponding Hamiltonian(1) is obtained as

$$\begin{aligned}\hat{H}^{[2],(\mathrm{N})} =& \frac{1}{2}\{G_{gg}\Pi_g^2 + F_{gg}S_g^2\} + \frac{1}{2}\{G_{uu}\Pi_u^2 + F_{uu}S_u^2\} \\ & - g_{aa}P_+P_- - f_{aa}Q_+Q_-,\end{aligned} \tag{77}$$

where the Fermi interaction is

$$\begin{aligned}\hat{V}_F^{(\mathrm{N})} =& -\frac{1}{\sqrt{2}}\left[\left(\frac{\partial g_{aa}}{\partial q_1}\right)_0 + \left(\frac{\partial g_{aa}}{\partial q_2}\right)_0\right]S_gP_+P_- + \frac{\gamma}{\sqrt{2}}S_uP_+P_- \\ & + \frac{1}{2\sqrt{2}}\left[\left(\frac{\partial g_{1a}}{\partial q_a}\right)_0 + \left(\frac{\partial g_{2a}}{\partial q_a}\right)_0\right][\Pi_g(Q_-P_- + Q_+P_+) + H.c.] \\ & - 2\sqrt{2}\frac{1}{3!}\frac{3!}{2!}[f_{1aa}S_gQ_+Q_-].\end{aligned} \tag{78}$$

This Hamiltonian in the algebraic representation takes the same expression of Eq. (4) when $\delta_{gu} = \alpha_u^{(\mathrm{L}')} = 0$

$$\hat{H}^{(\mathrm{N})} = \hbar\omega_g\ a_g^\dagger a_g + \hbar\omega_u\ a_u^\dagger a_u + \hbar\omega \sum_{\alpha=+,-} \tau_\alpha^\dagger\tau_\alpha + \alpha_F^{(\mathrm{N})}(a_g^\dagger\tau_+\tau_- + H.c.) \tag{79}$$

where, in this case, the Fermi parameter is

$$\begin{aligned}\alpha_F^{(\mathrm{N})} =& \frac{1}{2}\left(\frac{\partial g_{aa}}{\partial q_1}\right)_0 \hbar\omega\mu\sqrt{\frac{\hbar}{\omega_g\mu_g}} - \hbar\left(\frac{\partial g_{1a}}{\partial q_a}\right)_0\sqrt{\hbar\omega_g\mu_g} \\ & - \frac{1}{2!}\frac{\hbar}{\omega\mu}\sqrt{\frac{\hbar}{\omega_g\mu_g}}\ f_{1aa}.\end{aligned} \tag{80}$$

The fit using this Hamiltonian provides the spectroscopic parameters displayed in Table 19, while the estimation of the force constants are given in Table 20.

Table 19: Hamiltonian parameters in cm^{-1} fitted to the fundamentals as well as to the first bending overtone using the Hamiltonian (79).

Isotopologue	ω_g	ω	ω_u	α_F
(636)	1338.94	648.48	2283.48	-47.70
(626)	1338.83	667.31	2349.14	-51.35
(727)	1299.04	662.07	2330.60	-51.82
(828)	1262.76	657.32	2314.04	-52.30

Table 20: Force constants derived from the spectroscopic constants displayed in Table 19.

Isotopologue	$f_{11}^{(N)}(aJ\mathring{A}^{-2})$	$f_{12}^{(N)}(aJ\mathring{A}^{-2})$	$f_{aa}^{(N)}(aJ\mathring{A}^{-2})$	$f_{1aa}^{(N)}(aJ\mathring{A}^{-3})$
(636)	15.54	1.34	0.57	-0.88
(626)	15.53	1.35	0.57	-0.91
(727)	15.54	1.35	0.57	-0.94
(828)	15.55	1.35	0.57	-0.97
(626) Sánchez-Castellanos[100]	15.95	1.24	0.58	-0.96
(626) Chedin[72]	15.97	1.25	0.58	-0.88

Appendix C. Transformation of the local-normal bosonic operators in the limit for the symmetric isotopologues

Let us now carry out the analysis of the normal bosonic operators in terms of the bosonic local operators. Hence we proceed to obtain the limit for the symmetric isotopologues in the expression (24). In this case $\iota = \alpha$ and we have

$$\mathcal{A}_\alpha^\dagger = \sum_j (c_+^{\alpha,j} a_j^\dagger + c_-^{\alpha,j} a_j), \tag{81}$$

with

$$c_\pm^{\alpha,j} = \frac{1}{2\sqrt{2}}(-1)^{(\alpha+1)(1-\delta_{j1})}\beta_\alpha \sqrt{\frac{\hbar}{\omega_1\mu_1}}\left[(L^{-1})_{\alpha\alpha} \pm (\tilde{L})_{\alpha\alpha}\frac{\omega_1\mu_1}{\hbar\beta_\alpha^2}\right], \tag{82}$$

and explicitly

$$c_\pm^{\alpha,j} = \frac{1}{2\sqrt{2}}(-1)^{(\alpha+1)(1-\delta_{j1})}\left(\frac{g_{11}^{(0)}F_{\alpha\alpha}}{f_{11}G_{\alpha\alpha}^{(0)}}\right)^{1/4}\left[1 \pm \left(\frac{f_{11}G_{\alpha\alpha}^{(0)}}{g_{11}^{(0)}F_{\alpha\alpha}}\right)^{1/2}\right]. \tag{83}$$

where it has been considered that $\beta_\alpha^2 = \frac{1}{\hbar}\sqrt{F_{\alpha\alpha}/G_{\alpha\alpha}^{(0)}}$. In terms of the parameters x_g and x_f, this expression is recast in the form

$$c_\pm^{\alpha,j} = \frac{1}{2\sqrt{2}}(-1)^{(\alpha+1)(1-\delta_{j1})}\left(\frac{1+(-1)^{(\alpha+1)}x_f}{1+(-1)^{(\alpha+1)}x_g}\right)^{1/4}\left[1 \pm \left(\frac{1+(-1)^{(\alpha+1)}x_g}{1+(-1)^{(\alpha+1)}x_f}\right)^{1/2}\right], \tag{84}$$

with the correspondence $\alpha = 1 \rightarrow$ gerade and $\alpha = 2 \rightarrow$ ungerade. In Table 21 the coefficients $c_\pm^{\alpha,j}$ are displayed, where we notice again that the main contribution corresponds to the creation local operators.

Table 21: Table of coefficients $c_\pm^{\iota,j}$ involved in the expansion (24) for the symmetric isotopologues.

Isotopologue	α-th Mode	$c_+^{\alpha,1}$	$c_+^{\alpha,2}$	$c_-^{\alpha,1}$	$c_-^{\alpha,2}$	$\sum_j \lvert c_-^{\iota,j}\rvert^2$	δ_-
(636)	g	0.7133	0.7133	-0.0939	-0.0939	0.01767	0.03375
	u	0.7245	-0.7245	0.1578	- 0.1578	0.04982	
(626)	g	0.7136	0.7136	-0.0963	-0.0963	0.01855	0.03684
	u	0.7263	-0.7263	0.1660	-0.1660	0.05514	
(727)	g	0.7138	0.7138	-0.0979	-0.0979	0.01920	0.03933
	u	0.7278	-0.7278	0.1724	-0.1724	0.05945	
(828)	g	0.71407	0.71407	-0.09954	-0.09954	0.01981	0.04181
	u	0.7293	-0.7293	0.1786	- 0.1786	0.06380	

From (84) we obtain in a straightforward way the pure local limit

$$\lim_{x_f,x_g\to 0} c_+^{\alpha,j} = \frac{1}{\sqrt{2}}(-1)^{(\alpha+1)(1-\delta_{j1})}; \qquad \lim_{x_f,x_g\to 0} c_-^{\alpha,j} = 0, \tag{85}$$

and therefore

$$\mathcal{A}_\alpha^\dagger = \frac{1}{\sqrt{2}}[a_1^\dagger + (-1)^{(\alpha+1)}a_2^\dagger], \tag{86}$$

which corresponds to a canonical transformation, as expected.

Finally, it is convenient to present the components of the wave functions involved in the most important transition intensities for the Raman spectra. The results are presented in Table 22.

Table 22: Wave functions and transition energies (in cm^{-1}) involved in the most intense lines of the Raman spectrum. Because of the normalization of the states, the parameters a and a' determine the transition strength. The transition energies were taken from experimental results.

Symmetry	(636)	(626)	(727)	(828)	$\|\nu\rangle \to \|\nu'\rangle$
Σ_g^+	1265.83	1285.43	1258.17	1230.32	$\|00^00\rangle \to a\|10^00\rangle + b\|02^00\rangle$
Σ_g^+	1370.06	1388.28	1364.95	1347.09	$\|00^00\rangle \to b\|10^00\rangle - a\|02^00\rangle$
$\Pi_u^\pm$	1248.06	1265.09	1238.09	1211.37	$\|01^{\pm1}0\rangle \to a'\|11^{\pm1}0\rangle + b'\|03^{\pm1}0\rangle$
$\Pi_u^\pm$	1388.61	1409.48	1385.97	1367.2	$\|01^{\pm1}0\rangle \to b'\|01^{\pm1}0\rangle - a'\|03^{\pm1}0\rangle$
a	0.5587	0.6983	0.7826	0.8488	
a'	0.6076	0.7045	0.7586	0.8150	

References

[1] J-L. Bertaux, A.C. Vandaele, V. Wilquet, F. Montmessin, R. Dahoo, E. Villard, O. Korablev, A. Fedorova, First observation of 628 CO_2 isotopologue band at 3.3 μm in the atmosphere of Venus by solar occultation from Venus Express. *Icarus* **2008**, 195, 28.

[2] S.A. Tashkun, V.I. Perevalov, CDSD-4000: High-resolution, high-temperature carbon dioxide spectroscopic databank. *J.Quant. Spectrosc. and Radiat. Transf.* **2011** 112, 1403.

[3] S. Robert, Yu.G. Borkov, J. Vander Auwera, R. Drummond, A. Mahieux, V. Wilquet, A.C. Vandaele, V.I. Perevalov, S.A. Tashkun, J.L. Bertaux, Assignment and rotational analysis of new absorption bands of carbon dioxide isotopologues in Venus spectra. *J.Quant. Spectrosc. and Radiat. Transf.* **2013**, 114, 29.

[4] V. Wilquet, A. Mahieux, A.C. Vandaele, V.I. Perevalov, S.A. Tashkun, A. Fedorova, O. Korablev, F. Montmessin, R. Dahoo, J.-L. Bertaux, Line parameters for the 01111–00001 band of $^{12}C^{16}O^{18}O$ from SOIR measurements of the Venus atmosphere. *J.Quant. Spectrosc. and Radiat. Transf.* **2008**, 109, 895.

[5] G.L. Villanueva, M.J. Mumma, R.E. Novak, T. Heweagama, Identification of a new band system of isotopic CO_2 near 3.3 μm: Implications for remote sensing of biomarker gases on Mars. *Icarus* **2008**, 195, 34.

[6] R.E. Novak, M.J. Mumma, G.L. Villanueva, Measurement of the isotopic signatures of water on Mars; Implications for studying methane. *Planet. Space Sci.* **2011** 59, 163.

[7] P. Cermák, E.V. Korvelets, D. Mondelain, S. Kassi, V.I. Perevalov, A. Campargue, High sensitivity CRDS of CO_2 in the 1.74 μm transparency window. A validation test for the spectroscopic databases. *J.Quant. Spectrosc. and Radiat. Transf.* **2018** 207, 95.

[8] C.E. Miller, L.R. Brown, R.A. Toth, D.C. Benner, V. Malathy Devi, Spectroscopic challenges for high accuracy retrievals of atmospheric CO_2 and the Orbiting Carbon Observatory (OCO) experiment. *C.R. Physique* **2005** 6, 876.

[9] C.E. Miller, M.A. Montgomery, R.M. Onorato, C. Johnstone, T.P. McNicholas, B. Kovaric, L.R. Brown. Near infrared spectroscopy of carbon dioxide. (II): $^{16}O^{13}C^{16}O$ and $^{16}O^{13}C^{18}O$ line positions.*Journal of Molecular Spectroscopy* **2004**, 228, 355.

[10] T.K. Bauska, D. Baggenstos, E.J. Brook, A.C. Mix, S.A. Marcott, V.V. Petrenko, H. Shaeffer, J.P. Severinghaus, J.E. Lee, Carbon isotopes characterize rapid changes in atmospheric carbon dioxide during the last deglaciation. *Proc. Nat. Acad. Sci.* **2016**, 113.13, 3465.

[11] E.T. Sundkist, W.S. Broeker, *Proceedings of Chapman Conference on natural variations in carbon dioxide and the carbon cycle*, Tarpon springs, FL, January 9-13. 1984, Washington DC. American Geophysical Union Monograph Series 32.

[12] J.R. Ehleringer, N. Buchmann, I.B. Flanagan, Carbon isotope ratios in below ground carbon cycle processes. *Ecol. Appl.* **2000** 10.2, 412.

[13] J.S. Li, G. Durry, J. Cousin, L. Joly, B. Parvitte, P.H. Flamant, F. Gibert, V. Zéninari, Tunable diode laser measurement of pressure-induced shift coefficients of CO_2 around 2.05 μm for Lidar application. *J.Quant. Spectrosc. and Radiat. Transf.* **2011**, 112, 1411.

[14] P. Čermák, E.V. Karlovets, D. Mondelain, S. Kassi, V.I. Perevalov, A. Campargue, High sensitivity CRDS of CO_2 in the 1.74 μm transparency window. A validation test for the spectroscopic databases *J. Quant. Spectr. Rad. Trans.* **2018**, 207, 95.

[15] R.A. Toth, L.R. Brown, C.E. Miller, V.M. Devi, D.C. Benner, Self-broadened widths and shifts of $^{12}C^{16}O_2$: 4750–7000 cm^{-1}. *J. Mol.Spectrosc.* **2006**, 239, 243.

[16] R.A. Toth, L.R. Brown, C.E. Miller, V.M. Devi, D.C. Benner, Line strengths of $^{12}C^{16}O_2$: 4550–7000 cm^{-1}. *J. Mol.Spectrosc.* **2006**, 239, 221.

[17] R.A. Toth, L.R. Brown, C.E. Miller, V.M. Devi, D.C. Benner, Line positions and strengths of $^{16}O^{12}C^{18}O$, $^{18}O^{12}C^{18}O$ and $^{17}O^{12}C^{18}O$ between 2200 and 7000 cm^{-1}. *J. Mol.Spectrosc.* **2007**, 243, 43.

[18] R.A. Toth, L.R. Brown, C.E. Miller, V. Malathy, V.M. Devi, D.C. Benner. Spectroscopic database of CO_2 line parameters: 4300–7000 cm^{-1}. *J. Quant. Spectr. Rad. Trans.* **2008** 109, 906.

[19] B.M. Elliott, K. Sung, C.E. Miller, FT-IR spectra of ^{17}O-enriched CO_2 in the ν_3 region: High accuracy frequency calibration and spectroscopic constants for $^{16}O^{12}C^{17}O$, $^{17}O^{12}C^{17}O$, and $^{17}O^{12}C^{18}O$. *J.Mol. Spectrosc.* **2014**, 304, 1.

[20] B.M. Elliott, K. Sung, C.E. Miller, FT-IR spectra of ^{18}O-, and ^{13}C-enriched CO_2 in the ν_3 region: High accuracy frequency calibration and spectroscopic constants for $^{16}O^{12}C^{18}O$, $^{18}O^{12}C^{18}O$, and $^{16}O^{13}C^{16}O$. *J.Mol. Spectrosc.* **2015**, 312, 78.

[21] J. Mandin. Interpretation of the CO_2 absorption bands observed in the Venus infrared spectrum between 1 and 2.5 μu *J.Mol. Spectrosc.* **1977** 67, 304.

[22] B.V. Perevalov, V.I. Perevalov, A. Campargue. A (nearly) complete experimental linelist for $^{13}C^{16}O_2$, $^{16}O^{13}C^{18}O$, $^{16}O^{13}C^{17}O$, $^{13}C^{18}O_2$ and $^{17}O^{13}C^{18}O$ by high-sensitivity CW-CRDS spectroscopy between 5851 and 7045 cm[1]. *J.Quant. Spectrosc. and Radiat. Transf.* **2008**, 109, 2437.

[23] E.V. Karlovets, A. Campargue, D. Mondelain, S. Béguier, S. Kassi, S.A. Tashkun, V.I. Perevalov, High sensitivity Cavity Ring Down spectroscopy of 18O enriched carbon dioxide between 5850 and 7000 cm $^{-1}$ analysis and theoretical modeling of the $^{16}O^{12}C^{18}O$ spectrum. *J.Quant. Spectrosc. and Radiat. Transf.* **2013**, 130, 116.

[24] B.V. Perevalov, S. Kassi, V.I. Perevalov, S.A. Tashkun, A. Campargue. High sensitivity CW-CRDS spectroscopy of $^{12}C^{16}O_2$, $^{16}O^{12}C^{17}O$ and $^{16}O^{12}C^{18}O$ between 5851 and 7045 cm^{-1}: Line positions analysis and critical review of the current databases. *J. Mol. Spectrosc.* **2008**, 252, 143.

[25] S. Kassi, K.F. Song, A. Campargue. High sensitivity CW-cavity ring down spectroscopy of $^{12}CO_2$ near 1.35 μm (I): line positions. *J.Quant. Spectrosc. and Radiat. Transf.* **2009**, 110, 1801.

[26] K. Song, S. Kassi, S. Tashkun, V. Perevalov, A. Campargue. High sensitivity CW-cavity ring down spectroscopy of $^{12}CO_2$ near 1.35 μm (II): New observations and line intensities modeling. *J. Quant. Spectrosc. Radiat. Transf.* **2010** , 111, 332.

[27] E. Karlovets, S. Kassi, S. Tashkun, V. Perevalov, A. Campargue. High sensitivity Cavity Ring Down spectroscopy of carbon dioxide in the 1.19–1.26 μm region. *J. Quant. Spectrosc. Radiat. Transf.* **2014** 144, 137.

[28] T. Petrova, A. Solodov, D. Jaquemart, B. Borkov, O. Lyulin, Y. Borkov, S. Tashkun, V. Perevalov. Measurements of CO_2 line parameters in the 9250–9500 cm^{-1} and 10,700–10,860 cm^{-1} regions. *J. Quant. Spectrosc. Radiat. Transf.* **2015** 164, 109.

[29] Y. Tan, X.Q. Zhao, A.W. Liu, S.M. Hu, O. Lyulin, S. Tashkun, V. Perevalov. Cavity ring-down spectroscopy of CO_2 overtone bands near 830 nm. *J. Quant. Spectrosc. Radiat. Transf.* **2015**, 165, 22.

[30] A. Campargue, D. Bailly, J. Teffo, S. Tashkun, V. Perevalov. The $\nu_1 + 5\nu_3$ Dyad of $^{12}CO_2$ and $^{13}CO_2$. *J. Mol. Spectrosc.* **1999** 193, 204.

[31] G. Weireauch, G. Wumaier, A. Campargue, S. Tashkun, V. Perevalov, J. Teffo, The $2\nu_1 + 5\nu_3$ Triad of $^{12}CO_2$ *J. Mol. Spectrosc.* **1999** 198, 187.

[32] G. Weireauch, A. Campargue, Spectroscopy and Intensity Measurements of the $3\nu_1+3\nu_3$ Tetrad of $^{12}CO_2$ and $^{13}CO_2$. *J. Mol. Spectrosc.* **2001** 207, 263.

[33] Y. Ding, A. Campargue, E. Bertseva, S.A. Tashkun, V.I. Perevalov. Weireauch, A. Campargue, Highly sensitive absorption spectroscopy of carbon dioxide by ICLAS-VeCSEL between 8800 and 9530 cm^{-1} *J. Mol. Spectrosc.* **2005**, 231, 117.

[34] A. Garnache, A. Liu, L. Cerruti, A. Campargue. Intracavity laser absorption spectroscopy with a vertical external cavity surface emitting laser at 2.3 μm: Application to water and carbon dioxide. *Chem. Phys. Lett.* **2005**, 416, 22.

[35] Y. Ding, V.I. Perevalov, S.A. Tashkun, J.L. Teffo, A.W.Liu, S.M. Hu. Highly sensitive absorption spectroscopy of carbon dioxide by ICLAS-VeCSEL between 8800 and 9530 cm^{-1}. *J. Mol. Spectrosc.* **2003**, 220, 276.

[36] Y. Ding, P. Macko, D. Romanini, V.I. Perevalov, S.A. Tashkun, J.L. Teffo, S.M. Hu, A. Campargue, High sensitivity cw-cavity ringdown and Fourier transform absorption spectroscopies of $^{13}CO_2$. *J. Mol. Spectrosc.* **2004**, 226, 146.

[37] E.V. Karlovets, S.Kassi, S.A.Tashkun, P.I. Perevalov, A. Campargue, High sensitivity Cavity Ring Down spectroscopy of carbon dioxide in the 1.19–1.26 μm region. *J.Quant. Spectrosc. and Radiat. Transf.* **2014**, 144, 137.

[38] E.V. Karlovets,A. Campargue, A. Mondelain, S. Kassi, S.A. Tashkun, P.I. Perevalov, High sensitivity Cavity Ring Down spectroscopy of 18O enriched carbon dioxide between 5850 and 7000 cm^{-1}: Part III–Analysis and theoretical modeling of the $^{12}C^{17}O_2$, $^{16}O^{12}C^{17}O$, $^{17}O^{12}C^{18}O$, $^{16}O^{13}C^{17}O$ and $^{17}O^{13}C^{18}O$ spectra. *J.Quant. Spectrosc. Radiat. Transf.* **2014**, 136, 89.

[39] E.V. Karlovets, A. Campargue, A. Mondelain, S. Kassi, S.A. Tashkun, P.I. Perevalov. High sensitivity Cavity Ring Down spectroscopy of 18O enriched carbon dioxide between 5850 and 7000 cm^{-1}: Part II—Analysis and theoretical modeling of the $^{12}C^{18}O_2$, $^{13}C^{18}O_2$ and $^{16}O^{13}C^{18}O$ spectra. *J.Quant. Spectrosc. and Radiat. Transf.* **2014**, 136, 71.

[40] Y.G. Borkov, D. Yacquemart, O.M. Lyulin, S.A. Tashkun, P.I. Perevalov. Infrared spectroscopy of 17O- and 18O-enriched carbon dioxide: Line positions and intensities in the 3200–4700 cm^{-1} region. Global modeling of the line positions of $^{16}O^{12}C^{17}O$ and $^{17}O^{12}C^{17}O$. *J.Quant. Spectrosc. and Radiat. Transf.* **2014** 137, 57.

[41] A.G.E. Vaernewijck, S. Kassi, M. Herman. $^{17}O^{12}C^{17}O$ and $^{18}O^{12}C^{17}O$ overtone spectroscopy in the 1.64 μm region. *Chem. Phys. Lett.* **2011** 514, 29.

[42] K.F. Song, Y. Lu, Y. Tan, B. Gao, A.W. Liu, S.M.Hu. High sensitivity cavity ring down spectroscopy of CO_2 overtone bands near 790 nm. *J.Quant. Spectrosc. and Radiat. Transf.* **2011** 112, 761.

[43] V.I. Serdyukov, L.L. Sinitsa, A.A. Lugovskoi, Y.G. Borkov, S.A. Tashkun, V.I.Perevalov. LED-based Fourier transform spectroscopy of $^{16}O^{12}C^{18}O$ and $^{12}C^{18}O_2$ in the 11,260–11,430 cm^{-1} range. *J.Quant. Spectrosc. and Radiat. Transf.* **2016** 177, 145.

[44] X. de G. d'E. Vaernewijck, S. Kasssi, M. Herman. $^{17}O^{12}C^{17}O$ and $^{18}O^{12}C^{17}O$ overtone spectroscopy in the 1.64 μm region. *Chem. Phys. Lett.* **2011** 514, 29.

[45] X. de G. d'E. Vaernewijck, S. Kasssi, M. Herman. $^{17}O^{12}C^{17}O$ and $^{18}O^{12}C^{17}O$ spectroscopy in the 1.6 μm region. *Mol. Phys.* **2012** 110, 2665.

[46] S.N. Yurchenko, T.M. Mellor, R.S. Freedman, J. Tennyson. ExoMol line lists - XXXIX. Rovibrational molecular line list for CO_2. *Monthly Notices of the Royal Astronomical Society*, **2020**, 496, 5282.

[47] P. Kang, J. Wang, G.-L. Liu, Y.R. Sun, Z.-Y. Zhou, A.-W. Liu, S.-M. Hu. Line intensities of the 30011e – 00001e band of $^{12}C^{16}O_2$ by laser-locked cavity ring-down spectroscopy. *J. Quant. Spectr. Rad. Trans.* **2018**, 207, 1.

[48] E.V. Karlovets, A.D. Sidorenko, P. Cermák, D. Mondelain, S. Kassi, V.I. Perevalov, A. Campargue. The $^{13}CO_2$ absorption spectrum by CRDS near 1.74 m. *J. Mol. Spectrosc.* **2018**, 354, 54.

[49] E.V. Karlovets, P. Čermák, D. Mondelain, S. Kassi, A. Campargue, S.A. Tashkun, V.I. Perevalov, et al. Analysis and theoretical modeling of the ^{18}O enriched carbon dioxide spectrum by CRDS near 1.74 μm. *Journal of Quantitative Spectroscopy and Radiative Transfer* **2018**, 217, 73.

[50] E.V. Karlovets, I.E. Gordon, L.S. Rothman, R. Hashemi, R.J. Hargreaves, G.C. Toon, A. Campargue, V.I. Perevalov, P. Čermák, M. Birk, G. Wagner, J.T. Hodges, J. Tennyson, S.N. Yurchenko, The update of the line positions and intensities in the line list of carbon dioxide for the HITRAN2020 spectroscopic database. *Journal of Quantitative Spectroscopy and Radiative Transfer* **2021** 276, 107896.

[51] I.E. Gordon, L.S. Rothman, R.J. Hargreaves, R. Hashemi, E.V. Karlovets, F.M. Skinner, E.K. Conway, C. Hill, R.V. Kochanov, Y. Tan, *et. al.*, The HITRAN2020 molecular spectroscopic database. *Journal of Quantitative Spectroscopy and Radiative Transfer* **2022** 277, 107949.

[52] W. Gordy, R.L. Cook. Microwave Molecular Spectra. Part 2 of Chemical applications of spectroscopy, Interscience Pub., 1970.

[53] V.R. Stull, P.J. Wyatt, G.N. Plass. Vibrational Energies of the CO2 Molecule. *J. Chem. Phys.* **1962** 37, 1442.

[54] Z. Majcherova, P. Macko, D. Romanini, V.I. Perevalov, S.A. Tashkun,J.L. Teffo. High-sensitivity CW-cavity Ringdown Spectroscopy of (CO_2)-C-12 near 1.5 μm. *J. Mol. Spectrosc.* **2005** 230, 1.

[55] B.V. Perevalov, S.A. Tashkun, D. Romanini,V.I. Perevalov, S.A. Tushkun, A. Campargue. Global effective Hamiltonians of $^{16}O^{13}C^{17}O$ and $^{16}O^{13}C^{18}O$ improved from CW-CRDS observations in the 5900–7000 cm^{-1} region. *J. Mol. Spectrosc.* **2007**, 241, 90.

[56] V.I. Perevalov, S.A. Tashkun, K.F. Song, A. Campargue. Global modeling of $^{16}O^{12}C^{17}O$ and $^{16}O^{12}C^{18}O$ absolute line intensities in the 1.35 μm region. *J. Mol. Spectrosc.* **2010** 263, 183.

[57] A. Campargue, K.F. Song, N. Mouton, V.I. Perevalov, S. Kassi, High sensitivity CW-Cavity Ring Down Spectroscopy of five $^{13}CO_2$ isotopologues of carbon dioxide in the 1.26–1.44 μm region (I): Line positions.*Journal of Quantitative Spectroscopy and Radiative Transfer* **2010** 111, 659.

[58] E.V. Karlovets, A. Campargue, D. Mondelain, S.Kassi, S.A.Tashkun, V.I.Perevalov. High sensitivity Cavity Ring Down spectroscopy of 18O enriched carbon dioxide between 5850 and 7000 cm^{-1}: Part III–Analysis and theoretical modeling of the $^{12}C^{17}O_2$, $^{16}O^{12}C^{17}O$, $^{17}O^{12}C^{18}O$, $^{16}O^{13}C^{17}O$ and $^{17}O^{13}C^{18}O$ spectra *J.Quant. Spectrosc. and Radiat. Transf.* **2014**, 136, 89.

[59] J. Zúñiga, A. Bastida, M. Alacid, A. Requena. Variational Calculations of Rovibrational Energies for CO2. *J. Mol. Spectrosc.* **2001**, 205, 62.

[60] J.Cerezo, A.Bastida, A.Requena, J. Zúñiga. Rovibrational energies, partition functions and equilibrium fractionation of the CO2 isotopologues. *J.Quant. Spectrosc. and Radiat. Transf.* **2014**, 147, 233.

[61] R.B. Wattson, L.S. Rothman. Direct numerical diagonalization: Wave of the future. *J.Quant. Spectrosc. & Radiat. Transf.* **1992**, 48, 763.

[62] R.B. Wattson, L.S. Rothman. Determination of vibrational energy levels and parallel band intensities of 12C16O2 by Direct Numerical Diagonalization. *J. Mol. Spectrosc.* **1986**, 119, 83.

[63] M.B.E. Aguir, M.Y. Perrin, J. Taine. Variational Calculation of Energies of Highly Excited Rovibrational States of 12C16O2. *J. Mol. Spectrosc.* **2002**, 215, 234.

[64] E.J.Zak, J. Tennyson, O. L. Polyansky, L. Lodi, N. F. Zobov, S. A. Tashkun, V. I. Perevalov. Room temperature linelists for CO2 asymmetric isotopologues with ab initio computed intensities. *J.Quant. Spectrosc. & Radiat. Transf.* **2017**, 203, 265.

[65] X. Huang, D.W. Schwenke, S.A. Tashkun, T.J. Lee. An isotopic-independent highly accurate potential energy surface for CO2 isotopologues and an initial 12C16O2 infrared line list. *J.Chem.Phys.* **2012**, 136, 124311.

[66] Y. Lu, D. Xie, G.Yang. A potential energy surface for the electronic ground state of CO2. *Int. J. Quant. Chem.* **2000**, 78, 269.

[67] J. Zúñiga, M. Alacid, A. Bastida, F.J. Carvajal, A. Requena. Determination of a Potential Energy Surface for CO2 Using Generalized Internal Vibrational Coordinates. *J. Mol. Spectrosc.* **1999**, 195, 137.

[68] J. Zúñiga, A. Bastida, M. Alacid, A. Requena. Global potential energy surfaces for the CO2 and CS2 molecules. *Chem.Phys.Lett.* **1999**, 313, 670.

[69] J.M.L. Martin, P.R. Taylor, T.J. Lee. Accurate ab initio quartic force fields for the N2O and CO2 molecules. *Chem. Phys. Lett.* **1993**, 205, 535.

[70] R.J. Rakauskas, J.K. Šulskus, S.M. Zavoruev and V.A. Pivovar. The ab initio surfaces of the potential energy and dipole moment of $^1\Sigma_g^+$ CO_2. Stretching vibrational states. *Chem. Phys. Lett.* **1989**, 163, 381.

[71] H. Romanowski, R.B. Gerber, M.A. Ratner. The anharmonic stretching–bending potential of CO2 from inversion of spectroscopic data. *J. Chem.Phys.* **1988**, 88, 6757.

[72] A. Chedin, J.L.Teffo. The carbon dioxide molecule: A new derivation of the potential, spectroscopic, and molecular constants. *J. Mol. Spectrosc.* **1984**, 107, 333.

[73] A. Chedin. The carbon dioxide molecule: Potential, spectroscopic, and molecular constants from its infrared spectrum. *J. Mol. Spectrosc.* **1979**, 76, 430.

[74] M. Lacy. The anharmonic force field of carbon dioxide. *Mol. Phys.* **1982**, 45, 253.

[75] I. Suzuki. General anharmonic force constants of carbon dioxide. *J. Mol. Spectrosc.* **1982**, 45, 253.

[76] X. Huang, D.W. Schwenke, T.J. Lee. Isotopologue consistency of semi-empirically computed infrared line lists and further improvement for rare isotopologues: CO2 and SO2 case studies. *J.Quant. Spectrosc. & Radiat. Transf.* **2019**, 230, 222.

[77] X. Huang, D. W. Schwenke, R.S. Freedman, T.J.Lee. Ames-2016 line lists for 13 isotopologues of CO2: Updates, consistency, and remaining issues. *J.Quant. Spectrosc. & Radiat. Transf.* **2017**, 203, 224.

[78] C. Miller, L. Brown. Near infrared spectroscopy of carbon dioxide I. 16O12C16O line positions. *J. Mol. Spectrosc.* **2004**, 228, 329.

[79] A. Adel, D. M. Dennison. The Infrared Spectrum of Carbon Dioxide. Part I. *Phys. Rev.* **1933**, 43, 716.

[80] X. Huang, D.W. Schwenke, R.S. Freedman, T.J. Lee. Ames-2021 CO2 Dipole Moment Surface and IR Line Lists: Toward 0.1% Uncertainty for CO2 IR Intensities. *J. Phys. Chem. A* **2022**, 126, 5940.

[81] G. Herzberg *Molecular Spectra and Molecular Structure II. Infrared and Raman Spectra*, Florida, USA, (1945).

[82] K.J. Dennis, H.P. Affek, B.H. Passey, D.P. Schrag, J.M. Eiler. Defining an absolute reference frame for 'clumped' isotope studies of CO2. *Geochim. Cosmochim. Acta* **2011**, 75, 7117.

[83] X. Cao, Y. Liu. Theoretical estimation of the equilibrium distribution of clumped isotopes in nature. *Geochim. Cosmochim. Acta* **2012**, 77, 292.

[84] M.A. Webb, T.F. Miller. Position-Specific and Clumped Stable Isotope Studies: Comparison of the Urey and Path-Integral Approaches for Carbon Dioxide, Nitrous Oxide, Methane, and Propane. *J. Phys. Chem. A* **2014**, 118, 467.

[85] N. Yoshida, M. Vasilev, P. Ghosh, O. Abe, K. Yamada, M. Morimoto. Precision and long-term stability of clumped-isotope analysis of CO2 using a small-sector isotope ratio mass spectrometer. *Rapid Commun. Mass Spectrom.* **2013**, 27, 207.

[86] R.A. Eagle, E.A. Schuble, A.K. Tripati A,T. Tütken, R.C. Hulbert, J.M. Eiler. Body temperatures of modern and extinct vertebrates from 13C-18O bond abundances in bioapatite. *Proc. Natl. Acad. Sci.* **2010**, 107, 10377.

[87] L.Y. Yeung, H.P. Affek, J.K. Hoag, W. Guo, A. A. Wiegel, E.L. Atlas, S.M. Schauffler, M. Okumura, K.A. Boering, J.M. Eiler, Large and unexpected enrichment in stratospheric $^{16}O^{13}C^{18}O$ and its meridional variation. *Proc. Natl. Acad. Sci.* **2009**, 106, 11496.

[88] H.P. Affek, X. Xu, J.M. Eiler. Seasonal and diurnal variations of 13C18O16O in air: Initial observations from Pasadena, CA. *Geochim. Cosmochim. Acta.* **2007**, 71, 5033.

[89] H.P. Affek, J.M. Eiler. Abundance of mass 47 CO 2 in urban air, car exhaust, and human breath. *Geochim. Cosmochim. Acta.* **2006**, 70, 1.

[90] J.M. Eiler, E.A. Schauble. 18O13C16O in Earth's atmosphere. *Geochim. Cosmochim. Acta.* **2004**, 68, 4767.

[91] Z. Wang, E.A. Schauble, J.M. Eiler. Equilibrium thermodynamics of multiply substituted isotopologues of molecular gases. *Geochim. Cosmochim. Acta.* **2004**, 68, 4779.

[92] J. Santrock, S.A. Studley, J. Hayes. Isotopic analyses based on the mass spectrum of carbon dioxide. *Anal. Chem.* **1985**, 57, 1444.

[93] H. Huntington, J. Eiler, H.P. Affek, W. Guo, M. Bonifacie, L. Yeung, N. Thiagarajan, B. Passey, A. Tripati, M. Daëron, *et al.*, Methods and limitations of 'clumped' CO2 isotope (Δ_{47}) analysis by gas-source isotope ratio mass spectrometry. *J.Mass Spectrom.* **2009**, 44, 1318.

[94] J. Eiler, M. Clog, P.Magyar, A. Piasecki, A. Sessions, D. Stolper, M. Deerberg, H.J.Schlueter, J. Schwieters. A high-resolution gas-source isotope ratio mass spectrometer. *J.Mass Spectrom.* **2013**, 335, 45.

[95] A. Castrillo, G. Casa, L. Gianfrani. Oxygen isotope ratio measurements in CO2 by means of a continuous-wave quantum cascade laser at 4.3 μm *Optics Lett.* **2007**, 32, 3047.

[96] I. Prokhorov, T. Kluge, C. Janssen. Optical clumped isotope thermometry of carbon dioxide. *Scientific Reports.* **2019**, 9, 1.

[97] A.J. Fleisher, H. Yi, A. Strivastava, O.L. Polyansky, N.F. Zobov, J.T. Hodges. Absolute 13C/12C isotope amount ratio for Vienna PeeDee Belemnite from infrared absorption spectroscopy. *Nat. Phys.* **2021**, 9, 1.

[98] T. Sako,D. Aoki, K. Yamanouchi, F. Iachello. Algebraic force-field Hamiltonian expansion approach to linear polyatomic molecules. *J. Chem. Phys.*. **2000**, 113, 6063.

[99] M. Sánchez-Castellanos, R.Lemus, M.Carvajal, F.Pérez-Bernal. A novel connection between algebraic spectroscopic parameters and force constants in the description of vibrational excitations of linear triatomic molecules. *J. Mol. Spectrosc.* **2009**, 253, 1.

[100] M. Sánchez-Castellanos, R. Lemus, M. Carvajal, F. Pérez-Bernal. The potential energy surface of CO2 from an algebraic approach. *Int. J. Quant. Chem.* **2012**, 112, 3498.

[101] M. Bermúdez-Montaña, R. Lemus, F. Pérez-Bernal, M. Carvajal, Comprehensive vibrational analysis of CO2 based on a polyad-preserving model. *Eur. Phys. J. D* **2017**, 71, 147.

[102] M. Sánchez-Castellanos, R. Lemus, M. Carvajal, F. Pérez-Bernal, J.M. Fernández. A study of the Raman spectrum of CO2 using an algebraic approach. *Chem. Phys. Lett.* **2012**, 554, 208.

[103] R. Lemus, M. Sánchez-Castellanos, F. Pérez-Bernal, J.M. Fernández, M. Carvajal. Simulation of the Raman spectra of CO2: Bridging the gap between algebraic models and experimental spectra. *J. Chem. Phys.* **2014**, 141, 054306.

[104] A. R. Hoy, I. M. Mills, and G. Strey. Anharmonic force constant calculations. *Mol. Phys.*, **1972**, 24, 1265.

[105] M. M. Estévez-Fregoso, R. Lemus. Connection between the su(3) algebraic and configuration spaces: bending modes of linear molecules. *Mol. Phys.* **2018**, 116, 2374.

[106] M. Bermúdez-Montaña, M.Carvajal, F.Pérez-Bernal, R. Lemus. An algebraic alternative for the accurate simulation of CO2 Raman spectra. *J. Raman Spectroscopy* **2020**, 51, 569.

[107] M. Bermúdez Montaña, M. Rodríguez-Arcos, M.Carvajal, C. Ostertag-Henning, R. Lemus. Algebraic vibrational description of the symmetric isotopologues of CO2: (13)C(16)O2 , (12)C(18)O2 and (12)C(17)O2. *Chemical Physics* **2022**, 557, 111481.

[108] S.H. Dong, R. Lemus, A. Frank. Ladder operators for the Morse potential. *Int. J. Quant. Chem.* **2002**, 86, 433.

[109] R.D. Levine and C.F. Wulfman. Energy transfer to a morse oscillator. *Chem. Phys. Lett.*, **1979**, 60, 372.

[110] C.F. Wulfman, R.D. Levine. Isotopic substitution as a symmetry operation in molecular vibrational spectroscopy. *Chem. Phys. Lett.*, **1984**, 104, 9.

[111] O.S. van Roosmalen, I. Benjamin and R.D. Levine. A unified algebraic model description for interacting vibrational modes in ABA molecules. *J. Chem. Phys.* , **1984**, 81, 5986.

[112] F. Iachello and R.D. Levine, *Algebraic Theory of Molecules*, Oxford University Press, 1995.

[113] F. Iachello, S. Oss. Algebraic approach to molecular spectra: Two-dimensional problems. *J. Chem. Phys.*, **1996**, 104, 6956.

[114] E.B, Wilson Jr., J.C.Decius and P. C. Cross, *Molecular Vibrations. The theory of Infrared and Raman Spectra*. Dover Publications. New York. 1955.

[115] P.M. Morse. Diatomic Molecules According to the Wave Mechanics. II. Vibrational Levels. *Phys. Rev.*, **1929**, 34, 57.

[116] A. Matsumoto. Generalised matrix elements in discrete and continuum states for the Morse potential. *J. Phys. B. At. Mol. Opt. Phys.*, **1988**, 21, 2863.

[117] M.S.Child, R.T. Lawton. Local and normal vibrational states: a harmonically coupled anharmonic-oscillator model. *Faraday Discuss. Chem. Soc.* **1981**, 71, 273.

[118] M.S. Child, L. Halonen. Overtone Frequencies and Intensities in the Local Mode Picture. *Adv. Chem. Phys.* **1984**, 1, 1.

[119] L. Halonen. Local mode vibrations in polyatomic molecules. *Adv. Chem. Phys.* **1998**, 104, 41.

[120] P. Jensen. An introduction to the theory of local mode vibrations. *Mol. Phys.* **2000**, 104, 1253.

[121] L.Halonen, M.S. Child. Model stretching overtone eigenvalues for SF_6, WF_6, and UF_6. *J. Chem. Phys.* **1983**, 79, 559.

[122] L. Halonen, *Computational Molecular Spectroscopy*. Edited by P. Jensen and P. Bunker. John Wiley and Sons. 2000.

[123] M.Bermúdez-Montaña, R. Lemus, O.Castaños. Fidelity, entropy, and Poincaré sections as tools to study the polyad breaking phenomenon. *Euro. Phys. Lett.* **2016**, 116, 13001.

[124] M.Bermúdez-Montaña, R. Lemus, O.Castaños. Polyad breaking phenomenon associated with a local-to-normal mode transition and suitability to estimate force constants. *Mol. Phys.* **2017**, 115, 3076.

[125] E. Fermi. Über den ramaneffekt des kohlendioxyds. *Zeitschrift für Physik* **1931**, 71, 250.

[126] A. B. McCoy, E.L. Sibert III. Perturbative calculations of vibrational (J=0) energy levels of linear molecules in normal coordinate representations. *J. Chem. Phys.* **1991**, 95, 3476.

[127] R. Lemus. Potential Energy Surfaces Using Algebraic Methods Based on Unitary Groups. *Adv. Phys. Chem.* **2011**, 2011, Article ID 593872, 39 pp

[128] R.Lemus, M.Carvajal, J.C.López, A.Frank. Spectroscopic Description of H2O in the su(2) Vibron Model Approximation. *J.Mol.Spectrosc.* **2002**, 214, 52.

[129] R. Lemus. Vibrational excitations in H_2O in the framework of a local model. *J. Mol. Spectrosc.*, **2004**, 225, 73.

[130] R. Lemus, A. Frank. Vibrational Excitations of Methane in the Framework of a Local-Mode Anharmonic Model. *J. Mol. Spectrosc.* **2000**, 201, 198.

[131] M. Sánchez-Castellanos, C.A.Amezcua-Eccius, O.Álvarez-Bajo, R.Lemus. A local–normal description of vibrational excitations of pyramidal molecules in terms of Morse oscillators. *J. Mol. Spectrosc.* **2008**, 247, 140.

[132] C.A. Amezcua-Eccius, R. Lemus. An approach for the description of vibrational excitations: Application to $^{11}BF_3$. *J.Mol.Spectrosc.* **2010**, 260, 36.

[133] R. Bernal and R. Lemus. Algebraic local vibrational spectroscopic description of formaldehyde. *J. Mol. Spectrosc.* **2006**, 235, 218.

[134] M. Sánchez-Castellanos and R. Lemus. Force field constants for Formaldehyde obtained from an algebraic approach. *J. Mol. Spectrosc.* **2011**, 266, 1.

[135] R.Lemus, M.Sánchez-Castellanos. A study of vibrational excitations of HCN in the framework of an algebraic model. *Mol. Phys.* **2011**, 109, 2009.

[136] M. Bermúdez Montaña, R. Lemus. A study of vibrational excitations of ozone in the framework of a polyad preserving model of interacting Morse oscillators. *J.Molecular Spectrosc.* **2017**, 331, 89.

[137] L. Coello, R. Lemus. Vibrational description of the stretching modes of octahedral molecules: a local-to-normal mode transition criterion. *Mol. Phy.* **2021**, 119, 7.

[138] O. Álvarez-Bajo, M. Carvajal, F. Pérez-Bernal. An approach to global rovibrational analysis based on anharmonic ladder operators: Application to Hydrogen Selenide ($H_2^{80}Se$) *Chem. Phys.* **2012**, 392, 63.

[139] M. Carvajal, R. Lemus. Toward a Global Analysis Method Based on Anharmonic Ladder Operators: Application to Hydrogen Sulfide ($H_2^{32}S$). *J. Phys. Chem. A*, **2015**, 119, 12823.

[140] D.H.Rank, A.G.St Pierre, T.A. Wiggins. Rotational and vibration constants of CO. *J. Mol. Spectrosc.* **1965**, 18, 418.

[141] J-Q. Chen, *Group representation theory for physicists*. World Scientific. New York. 1989.

[142] R.Lemus. A general method to obtain vibrational symmetry adapted bases in a local scheme. *Mol.Phys.* **2003**, 101, 2511.

[143] O. Álvarez-Bajo, R. Lemus, M. Carvajal, F. Pérez-Bernal. Equivalent rotations associated with the permutation inversion group revisited: symmetry projection of the rovibrational functions of methane. *Molecular Physics* **2011**, 109, 797.

[144] R.Lemus. Quantum Numbers and the Eigenfunction Approach to Obtain Symmetry Adapted Functions for Discrete Symmetries. *Symmetry* **2012**, 4, 667.

[145] L. Walters, The p-shell nuclei in a (0 + 2)/x model space, Ph.D. Thesis. University of Rijks, Groningen (1989).

[146] P.J. Brussaard, P.W.M. Glandemans, Shell-model applications in Nuclear Spectroscopy, North-Holland, Amsterdam, 1977.

[147] Y.G. Borkov, D. Jacquemart, O.M. Lyulin, S.A. Tashkun, V.I. Perevalov, Infrared spectroscopy of ^{17}O-and ^{18}O-enriched carbon dioxide: Line positions and intensities in the 4681–5337 cm^{-1} region. *Journal of Quantitative Spectroscopy and Radiative Transfer* **2015**, 159, 1.

[148] C. Claveau, J.-L. Teffo, D. Hurtmans, A. Valentin, Infrared fundamental and first hot bands of O^{12}C^{17}O isotopic variants of carbon dioxide. *Journal of molecular spectroscopy* **1998**, 189, 153.

[149] E.V. Karlovets, S. Kassi, A. Campargue. High sensitivity CRDS of CO_2 in the 1.18 μm transparency window. Validation tests of current spectroscopic databases. *Journal of Quantitative Spectroscopy and Radiative Transfer* **2020** 247, 106942.

[150] S. Vasilchenko, M. Konefal, D. Mondelain, S. Kassi, P. Čermák, S.A. Tashkun, V.I. Perevalov, A. Campargue, The CO_2 absorption spectrum in the 2.3 μm transparency window by high sensitivity CRDS:(I) Rovibrational lines. *Journal of Quantitative Spectroscopy and Radiative Transfer* **2016**, 184, 233.

[151] L. Wang, V.I. Perevalov, S.A. Tashkun, K.-F. Song, S.-M. Hu, Fourier transform spectroscopy of $^{12}C^{18}O_2$ and $^{16}O^{12}C^{18}O$ in the 3800–8500 cm $^{-1}$ region and the global modeling of the absorption spectrum of $^{12}C^{18}O_2$. *Journal of Molecular Spectroscopy* **2008** 247, 64.

[152] H. Pan, X.-F. Li, Y. Lu, A.-W. Liu, V.I. Perevalov, S.A. Tashkun, S.-M. Hu, Cavity ring down spectroscopy of ^{18}O and ^{17}O enriched carbon dioxide near 795 nm. *Journal of Quantitative Spectroscopy and Radiative Transfer* **2013** 114, 42.

[153] D. Golebiowski, M. Herman, O. Lyulin, $^{16}O^{12}C^{17}O$ and $^{18}O^{12}C^{17}O$ spectroscopy in the 1.2–1.25 μm region. *Canadian Journal of Physics* **2013**, 91, 963.

[154] S. Kassi, E.V. Karlovets, S.A. Tashkun, V.I. Perevalov, A. Campargue, Analysis and theoretical modeling of the 18O enriched carbon dioxide spectrum by CRDS near 1.35 μm: (I) $^{16}O^{12}C^{18}O$, $^{16}O^{12}C^{17}O$, $^{12}C^{16}O_2$ and $^{13}C^{16}O_2$. *Journal of Quantitative Spectroscopy and Radiative Transfer* **2017**, 187, 414.

[155] D. Mondelain, E.V. Karlovets, V.I. Perevalov, S.A. Tashkun, A. Campargue, High-sensitivity CRDS absorption spectrum of ^{17}O enriched carbon dioxide near 1.74 μm. *Journal of Molecular Spectroscopy* **2019** 362, 84.

[156] O.M. Lyulin, E.V. Karlovets, D. Jacquemart, Y. Lu, A.W. Liu, V.I. Perevalov, Infrared spectroscopy of ^{17}O-and ^{18}O-enriched carbon dioxide in the 1700–8300 cm^{-1} wavenumber region. *Journal of Quantitative Spectroscopy and Radiative Transfer* **2012**, 113, 2167.

[157] L.S. Rothman, R.L. Hawkins, R.B. Wattson, R.R. Gamache, Energy levels, intensities, and linewidths of atmospheric carbon dioxide bands. *Journal of quantitative spectroscopy and radiative transfer* **1992**, 48, 537.

[158] E.V. Karlovets, A. Campargue, S. Kassi, S.A. Tashkun, V.I. Perevalov, Analysis and theoretical modeling of ^{18}O enriched carbon dioxide spectrum by CRDS near 1.35 μm:(II) $^{16}O^{13}C^{18}O$, $^{16}O^{13}C^{17}O$, $^{12}C^{18}O_2$, $^{17}O^{12}C^{18}O$, $^{12}C^{17}O_2$, $^{13}C^{18}O_2$ and $^{17}O^{13}C^{18}O$. *Journal of Quantitative Spectroscopy and Radiative Transfer* **2017**, 191, 75.